

**METASTABILITY FOR A GENERALIZED BURGERS EQUATION  
WITH APPLICATIONS TO PROPAGATING FLAME-FRONTS**

Xiaodi Sun and Michael J. Ward<sup>1</sup>

*Department of Mathematics, University of British Columbia  
Vancouver, B.C. V6T 1Z2, Canada*

**Abstract**

In the small diffusion limit  $\varepsilon \rightarrow 0$ , metastable dynamics is studied for the generalized Burgers problem

$$\begin{aligned} u_t + f'(u)u_x - f''(u) &= \varepsilon u_{xx}, & 0 < x < 1, & \quad t > 0 \\ u(0, t) &= u(1, t) = 0, & u(x, 0) &= u_0(x). \end{aligned}$$

Here  $u = u(x, t)$  and  $f(u)$  is smooth, convex, and satisfies  $f(0) = f'(0) = 0$ . The choice  $f(u) = u^2/2$  has been shown previously to arise in connection with the physical problem of upward flame-front propagation in a vertical channel in a particular parameter regime. In this context, the shape  $y = y(x, t)$  of the flame-front interface satisfies  $u = -y_x$ . For this problem, it is shown that the principal eigenvalue associated with the linearization around an equilibrium solution corresponding to a parabolic-shaped flame-front interface is exponentially small. This exponentially small eigenvalue then leads to a metastable behavior for the time-dependent problem. This behavior is studied quantitatively by deriving an asymptotic ordinary differential equation characterizing the slow motion of the tip location of a parabolic-shaped interface. Similar metastability results are obtained for more general  $f(u)$ . These asymptotic results are shown to compare very favorably with full numerical computations.

## 1 Introduction

To study the dynamics of an upwardly propagating flame-front in a vertical channel, a nonlinear evolution equation for the flame-front interface was derived in [13] using a weak thermal expansion approximation. In a particular parameter regime and under various physical assumptions, the dimensionless flame-front interface  $y = y(x, t)$  was found to satisfy (see [13])

$$y_t - \frac{1}{2}y_x^2 = \varepsilon y_{xx} + y - \int_0^1 y dx, \quad 0 < x < 1, \quad t > 0, \quad (1.1a)$$

$$y_x(0, t) = 0, \quad y_x(1, t) = 0; \quad y(x, 0) = y_0(x). \quad (1.1b)$$

Here  $\varepsilon > 0$  is a small parameter. To study (1.1) it is convenient to re-formulate this problem in terms of the slope  $u(x, t) = -y_x(x, t)$ , which yields

$$u_t + uu_x - u = \varepsilon u_{xx}, \quad 0 < x < 1, \quad t > 0, \quad (1.2a)$$

---

<sup>1</sup>This work was supported by NSERC grant 5-81541

$$u(0,t) = u(1,t) = 0, \quad u(x,0) = u_0(x). \quad (1.2b)$$

As shown numerically in [12], the solution to (1.1) (or (1.2)), for a certain class of initial conditions relevant to flame–front propagation, exhibits a phenomenon known as dynamic metastability when  $\varepsilon \ll 1$ . In Fig. 1 we illustrate this metastable behavior by plotting some numerical results for the shape of the interface  $y = y(x,t)$  versus  $x$  at four different values of  $t$  when  $\varepsilon = 0.0115$ . In Fig. 1a we choose an initial condition where the flame–front assumes a somewhat concave parabolic shape. Then, as shown in Fig. 1a–c, the tip location  $x_0 = x_0(t)$  of the parabola, defined as the location of the maximum value of  $y$  at time  $t$ , moves towards the channel wall at  $x = 0$  rather slowly. For other initial conditions, the tip of this interface can move slowly towards the other wall at  $x = 1$ . When  $\varepsilon$  is decreased, this stage of the motion, whereby the tip of the parabolic flame–front moves towards one of the walls, becomes exceedingly slower than in Fig. 1a–c. In [4] it was proved that this motion is asymptotically exponentially slow as  $\varepsilon \rightarrow 0$ . Finally, when the tip of the interface comes close enough to the wall, the rate of evolution of the flame–front increases and a final equilibrium state is attained when the tip touches the wall (see Fig. 1c–d).

For the equilibrium problem, it was shown in [4] that (1.2) admits multiple equilibrium solutions when  $\varepsilon \ll 1$ . In particular, there exists a unique positive equilibrium  $U_\varepsilon^+$  and a unique negative equilibrium  $U_\varepsilon^-$ . These solutions were found to be linearly stable. In addition, for  $\varepsilon \ll 1$ , it was shown that (1.2) has two unstable equilibrium solutions  $U_{\varepsilon,1}^+$  and  $U_{\varepsilon,1}^-$ , which each have exactly one zero–crossing in the interval  $(0,1)$ . Other equilibrium solutions with more than one zero–crossing are also possible. The stability of these equilibrium solutions with more than one zero–crossing and the associated time–dependent solutions were studied in [8]. In Fig. 2 we plot the four equilibrium solutions  $U_\varepsilon^+$ ,  $U_\varepsilon^-$ ,  $U_{\varepsilon,1}^+$  and  $U_{\varepsilon,1}^-$  when  $\varepsilon = 0.005$ . From this figure we observe that  $U_\varepsilon^+$  and  $U_\varepsilon^-$  have boundary layers of width  $O(\varepsilon)$  near one of the endpoints,  $U_{\varepsilon,1}^+$  has an internal layer of width  $O(\varepsilon)$  near  $x = 1/2$ , and  $U_{\varepsilon,1}^-$  has an  $O(\varepsilon)$  boundary layer near each endpoint. Among these solutions,  $U_{\varepsilon,1}^-$  corresponds to a concave parabolic–shaped equilibrium flame–front interface. We show that the linearization of (1.2) around  $U_{\varepsilon,1}^-$  has an exponentially small principal eigenvalue as  $\varepsilon \rightarrow 0$ . Thus, it is this equilibrium solution that is the most significant for the occurrence of metastable behavior for the time–dependent problem.

For the time–dependent problem, our numerical computations and the results in [12] and [4] suggest that the occurrence of metastable behavior for (1.2) strongly depends on the initial condition. In particular, from [4], a sufficient condition for metastable flame–front dynamics for (1.2) (or equivalently (1.1)) is that the initial data  $u_0(x)$  satisfies

$$u_0(x) < 0 \quad \text{for } x \in (0, a), \quad \text{and} \quad u_0(x) > 0 \quad \text{for } x \in (a, 1), \quad (1.3)$$

where  $a > 0$ . For other cases, our numerical computations suggest that a stable equilibrium configuration can usually be attained in an  $O(1)$  time interval. In Fig. 3–5 we illustrate the dynamics of the solution  $u$  to

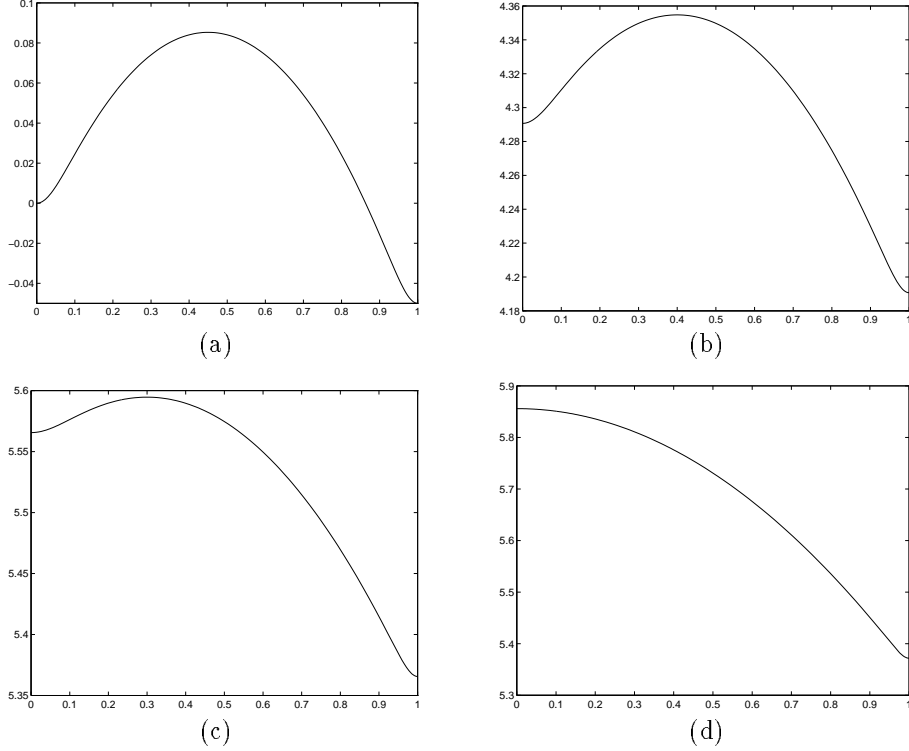


Figure 1: Plots of  $y(x, t)$  versus  $x$  with  $\varepsilon = .0115$  obtained from (5.5). (a) initial quasi-equilibrium solution  $y(x, t)$  with tip location  $x_0 = 0.45$  at  $t = 0$ ; (b) quasi-equilibrium solution with  $x_0 = 0.4$  at  $t = 90.05$ ; (c) quasi-equilibrium solution with  $x_0 = 0.3$  at  $t = 113.69$ ; (d) final stable equilibrium solution at  $t \geq 117.07$ .

(1.2) for various initial conditions. Only in Fig. 3, where the initial data satisfies (1.3), is an exponentially slow motion observed.

Therefore, when the initial data satisfies (1.3) and when  $\varepsilon \ll 1$ , we have three different time behaviors under (1.1): a transient  $O(1)$  phase where the parabolic-shaped flame-front interface is formed; an exponentially slow phase where the tip of the parabolic flame-front drifts towards one of the walls; an  $O(1)$  collapse phase where the flame-front collapses against the wall and attains its equilibrium configuration. In terms of  $u(x, t)$ , the first two phases are clearly seen in Fig. 3. The fact that the time interval corresponding to the second phase may become exceptionally long when  $\varepsilon$  is small creates an illusion that the flame-front has reached some final equilibrium. However, this phase is merely a quasi-equilibrium transient phase that persists for an exponentially long time interval. We remark that similar metastable behavior has previously been studied for viscous shock problems (cf. [10], [14]) and for phase-transition

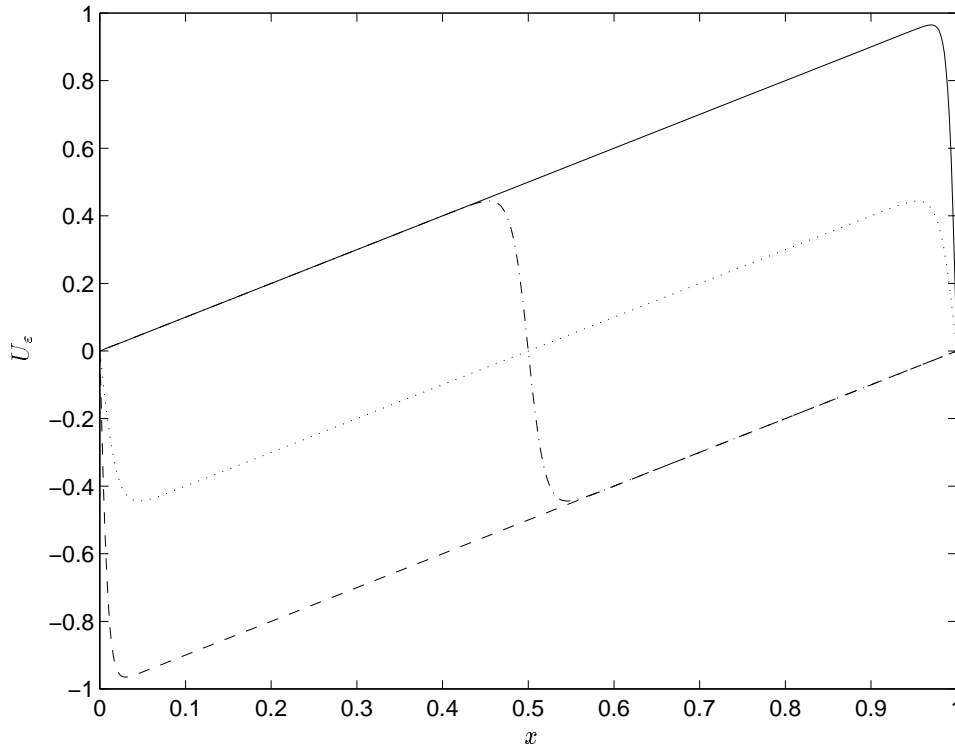


Figure 2: Plot of four equilibrium solutions  $U(x)$  versus  $x$  for (1.2) with  $\varepsilon = 0.005$ ,. The solid line and the dashed line represent the positive equilibrium  $U_\varepsilon^+$  and the negative equilibrium  $U_\varepsilon^-$ , respectively. The dotted line and the dash-dotted line show two unstable equilibrium  $U_{\varepsilon,1}^-$  and  $U_{\varepsilon,1}^+$ . The solution  $U_{\varepsilon,1}^-$  is closely related to the metastable parabolic-shaped flame front.

problems (cf. [5], [6], [15]). For a survey of metastable behavior in other contexts see [16].

One of our main goals is to use the projection method, developed previously in [14] and [15], to give an explicit asymptotic characterization of metastable flame-front motion for (1.1), (1.2) in the limit  $\varepsilon \rightarrow 0$ . The asymptotic results complement the rigorous, but qualitative, metastability result obtained in [4]. Using the method of matched asymptotic expansions, a quasi-steady concave parabolic-shaped flame-front interface for (1.1) can be expressed in terms of  $u(x, t)$  as  $u(x, t) \sim \tilde{u}^\varepsilon[x; x_0(t)]$ , where

$$\tilde{u}^\varepsilon[x; x_0] \equiv x - x_0 + u_l[\varepsilon^{-1}x; x_0] + u_r[\varepsilon^{-1}(1-x); x_0]. \quad (1.4)$$

Here  $u_l(y; x_0)$  and  $u_r(y; x_0)$  are boundary layer functions that tend to zero exponentially as  $y \rightarrow \infty$ , and the unknown  $x_0$  satisfies  $x_0 \in (0, 1)$ . Thus, to within exponentially small terms,  $x_0$  is the zero of  $u$ . Since  $y_x = -u$ , it follows that  $x_0 = x_0(t)$  also represents the trajectory of the tip of the parabolic-shaped

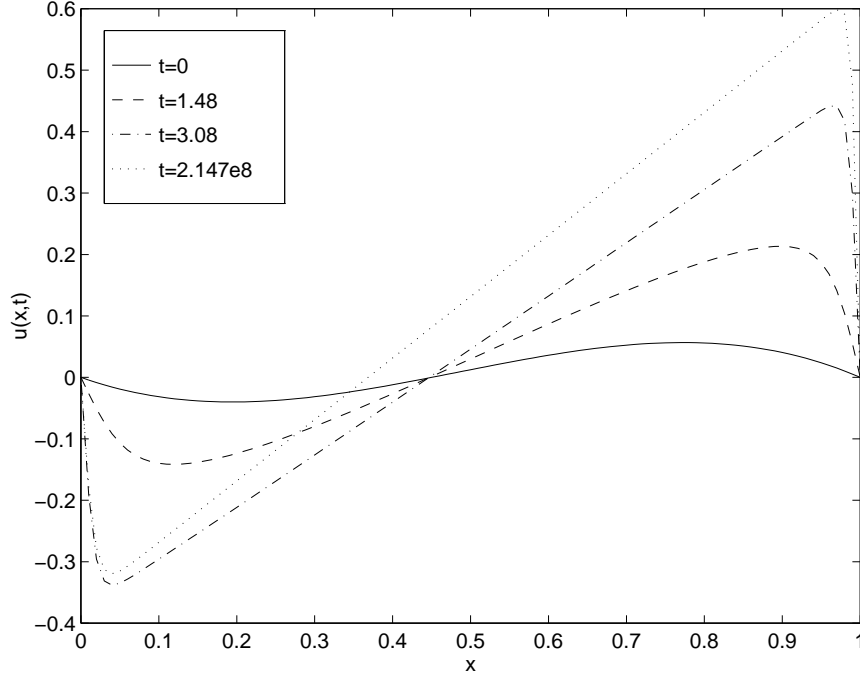


Figure 3: Plot of the solution to (1.2) at various times with  $\varepsilon = 0.003$ ,  $x_0^0 = 0.45$ , and initial data  $u(x, 0) = x(1 - x)(x - x_0^0)$ . Notice that the zero of  $u$ , which is the tip of the parabolic flame-front interface, moves slowly towards the wall at  $x = 0$ .

flame-front interface for (1.1). For a fixed  $x_0$  satisfying  $x_0 \in (0, 1)$ , we show that the principle eigenvalue associated with the linearization of (1.2) around  $\tilde{u}^\varepsilon$  is exponentially small and has the asymptotic estimate

$$\lambda_0 \sim \frac{1}{\varepsilon} \left[ x_0 \left( x_0 - c\varepsilon^{1/2} \right) e^{-x_0^2/2\varepsilon} + (1 - x_0) \left( (1 - x_0) - c\varepsilon^{1/2} \right) e^{-(1-x_0)^2/2\varepsilon} \right], \quad (1.5)$$

as  $\varepsilon \rightarrow 0$ , where  $c = (8/\pi)^{1/2}$ . This eigenvalue is responsible for the metastable behavior.

For the time-dependent problem, we use the projection method to derive an asymptotic ordinary differential equation for  $x_0(t)$ , which explicitly characterizes the metastable flame-front motion. This method is based on a quasi-steady linearization of (1.2) around  $\tilde{u}^\varepsilon$  given in (1.4). Since  $\lambda_0$  is exponentially small, a limiting solvability condition must hold in the limit  $\varepsilon \rightarrow 0$  for the linearized problem. From this condition, we will derive that  $x_0(t)$  satisfies

$$x_0' \sim \sqrt{\frac{2}{\pi\varepsilon}} \left[ \left( (1 - x_0)^2 + \frac{\pi^2\varepsilon}{3} \right) e^{-(1-x_0)^2/2\varepsilon} - \left( x_0^2 + \frac{\pi^2\varepsilon}{3} \right) e^{-x_0^2/2\varepsilon} \right]. \quad (1.6)$$

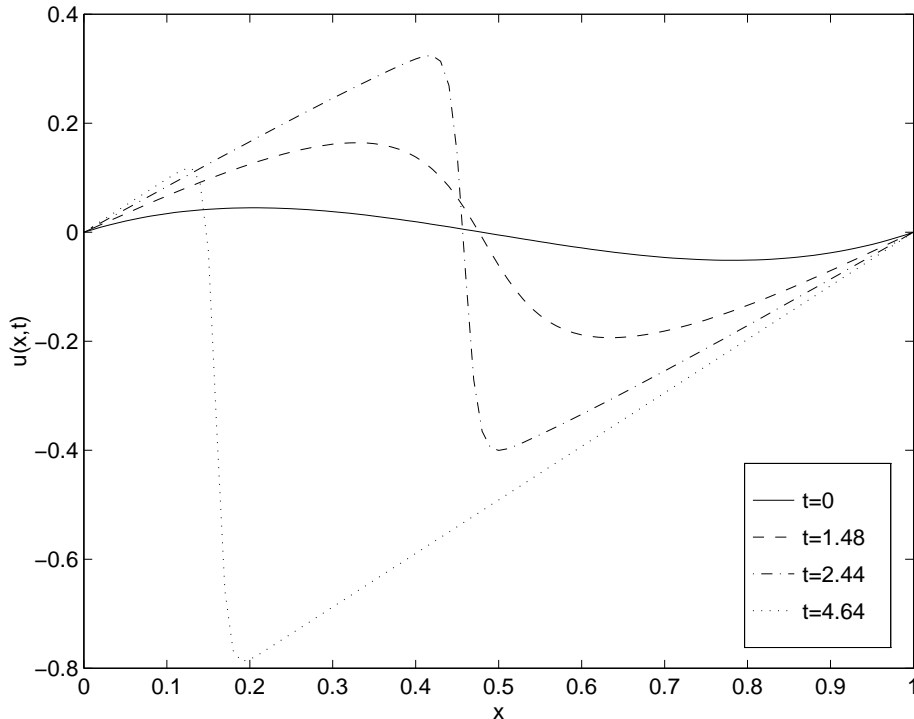


Figure 4: Plot of the solution to (1.2) at various times with  $\varepsilon = 0.003$ ,  $x_0^0 = 0.48$ , and initial data  $u(x, 0) = -x(1-x)(x-x_0^0)$ . A shock-layer is formed in an  $O(1)$  time interval and no metastable behavior is observed.

Rather than focusing exclusively on (1.2), we instead analyze the following generalized form of (1.2):

$$u_t + f'(u)u_x - f''(u) = \varepsilon u_{xx}, \quad 0 < x < 1, \quad t > 0, \quad (1.7a)$$

$$u(0, t) = u(1, t) = 0; \quad u(x, 0) = u_0(x). \quad (1.7b)$$

Here  $f(u)$  is smooth, convex, and satisfies  $f(0) = f'(0) = 0$ . The special case  $f(u) = u^2/2$  yields (1.2). This generalized problem exhibits a very similar metastable behavior as that for (1.2) and is no more difficult to analyze.

The outline of this paper is as follows. In §2, we construct an asymptotic expansion for a certain equilibrium solution of (1.7) and we outline the projection method. In §3 we derive a two-term asymptotic expansion for the principal eigenvalue  $\lambda_0$  associated with the corresponding linearized problem and we compare this expansion with full numerical results for  $\lambda_0$ . In §4, the asymptotic projection method is used

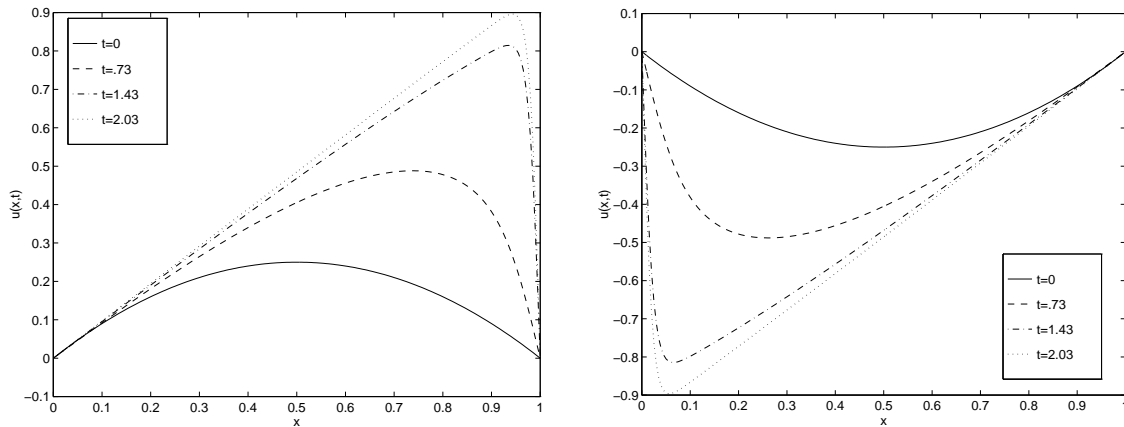


Figure 5: Plot of the solutions to (1.2) at various times with  $\varepsilon = 0.01$  and initial data  $u(x, 0) = x(1 - x)$ , (left figure) and  $u(x, 0) = -x(1 - x)$ , (right figure). Metastable behavior does not occur for these initial data.

to derive an ordinary differential equation characterizing the metastability in (1.7). In §5, we use a full numerical method to compute metastable behavior for (1.7) and we show how to recover the flame-front interface  $y(x, t)$  satisfying (1.1). The numerical results are found to compare very favorably with the corresponding asymptotic results in §4.

## 2 The Equilibrium Problem and the Projection Method

We first consider the equilibrium problem for (1.7) in the limit  $\varepsilon \rightarrow 0$

$$\varepsilon u_{xx} - f'(u)u_x + f'(u) = 0, \quad 0 < x < 1, \quad (2.1a)$$

$$u(0) = 0, \quad u(1) = 0. \quad (2.1b)$$

Here  $f(u)$  is smooth, convex, and satisfies  $f(0) = f'(0) = 0$ . This problem admits multiple equilibria. However, we will only construct a solution to (2.1) having the form given in (1.4), since it is this solution that is closely related to metastable behavior in the corresponding time-dependent problem.

The outer approximation for this solution is clearly  $u \sim x - x_0$  for some  $x_0 \in (0, 1)$ . This outer solution satisfies the differential equation (2.1a) exactly, but not the boundary conditions (2.1b). Therefore, there are boundary layers near the end points  $x = 0$  and  $x = 1$ . In the boundary layer near  $x = 0$  we let  $y = \varepsilon^{-1}x$  and  $u_l(y) = u(\varepsilon y)$ , and we expand

$$u_l(y) = -x_0 + u_{l_0}(y) + \varepsilon[y + u_{l_1}(y)] + \dots \quad (2.2)$$

Substituting (2.2) into (2.1), collecting powers of  $\varepsilon$ , and matching to the outer solution, we obtain

$$u_{l_0}'' - f'(-x_0 + u_{l_0})u_{l_0}' = 0, \quad 0 < y < \infty, \quad (2.3a)$$

$$u_{l_0}(0) = x_0, \quad u_{l_0}(y) \sim a_{l_0} e^{-\nu_l y} \quad \text{as } y \rightarrow \infty, \quad (2.3b)$$

and

$$u_{l_1}'' - [f'(-x_0 + u_{l_1})u_{l_1}]' = y f''(-x_0 + u_{l_1})u_{l_1}', \quad 0 < y < \infty, \quad (2.4a)$$

$$u_{l_1}(0) = 0, \quad u_{l_1}(y) \sim a_{l_1} y^2 e^{-\nu_l y} + b_{l_1} y e^{-\nu_l y} \quad \text{as } y \rightarrow \infty. \quad (2.4b)$$

Here  $a_{l_1} = f''(-x_0)a_{l_0}/2$  and  $b_{l_1} = 2a_{l_1}/\nu_l$ . Upon integrating (2.3), we find that the positive constants  $\nu_l$  and  $a_{l_0}$  are given by

$$\nu_l = -f'(-x_0), \quad (2.5a)$$

$$\log a_{l_0} = \log x_0 - \nu_l \int_{-x_0}^0 \left[ \frac{1}{f(s) - f(-x_0)} - \frac{1}{f'(-x_0)(s + x_0)} \right] ds. \quad (2.5b)$$

The asymptotic form in (2.4b) is obtained from (2.4a) by using the far-field behavior of  $u_{l_0}(y)$  as  $y \rightarrow \infty$ . By integrating (2.3) we obtain the equivalent first order equation

$$u_{l_0}' = f(u_{l_0} - x_0) - f(-x_0), \quad u_{l_0}(0) = x_0, \quad \text{with } u_{l_0}'(0) = -f(-x_0). \quad (2.6)$$

Similarly, in the boundary layer near  $x = 1$  we let  $y = \varepsilon^{-1}(1 - x)$  and  $u_r(y) = u(1 - \varepsilon y)$ , and we expand

$$u_r(y) = 1 - x_0 + u_{r_0}(y) + \varepsilon[u_{r_1}(y) - y] + \dots. \quad (2.7)$$

From (2.7) and (2.1) we obtain the boundary layer equations

$$u_{r_0}'' + f'(1 - x_0 + u_{r_0})u_{r_0}' = 0, \quad 0 < y < \infty, \quad (2.8a)$$

$$u_{r_0}(0) = x_0 - 1 < 0, \quad u_{r_0}(y) \sim -a_{r_0} e^{-\nu_r y} \quad \text{as } y \rightarrow \infty, \quad (2.8b)$$

and

$$u_{r_1}'' + [f'(1 - x_0 + u_{r_0})u_{r_1}]' = y f''(1 - x_0 + u_{r_0})u_{r_0}', \quad 0 < y < \infty, \quad (2.9a)$$

$$u_{r_1}(0) = 0, \quad u_{r_1}(y) \sim a_{r_1} y^2 e^{-\nu_r y} + b_{r_1} y e^{-\nu_r y} \quad \text{as } y \rightarrow \infty. \quad (2.9b)$$

Here  $a_{r_1} = -f''(1 - x_0)a_{r_0}/2$  and  $b_{r_1} = 2a_{r_1}/\nu_r$ . In (2.8b) the positive constants  $a_{r_0}$  and  $\nu_r$  are defined by

$$\nu_r = f'(1 - x_0), \quad (2.10a)$$

$$\log a_{r_0} = \log(1 - x_0) + \nu_r \int_0^{1-x_0} \left[ \frac{1}{f(1-x_0) - f(s)} + \frac{1}{f'(1-x_0)(s - 1 + x_0)} \right] ds. \quad (2.10b)$$

The first order equation equivalent to (2.8) is

$$u'_{r_0} = -f'(1 - x_0 + u_{r_0}) + f'(1 - x_0), \quad u_{r_0}(0) = x_0 - 1, \quad \text{with } u'_{r_0}(0) = f(1 - x_0). \quad (2.11)$$

Consider the left boundary layer expansion (2.2). Using the asymptotic behavior of  $u_{l_0}$  and  $u_{l_1}$  as  $y \rightarrow \infty$ , we observe that (2.2) becomes disordered (i.e.,  $\varepsilon u_{l_1} \ll u_{l_0}$  doesn't hold) as  $y \rightarrow \infty$  when  $\varepsilon y^2 = O(1)$  or, equivalently, when  $x = O(\varepsilon^{1/2})$ . Thus, (2.2) holds on the interval  $y = O(\varepsilon^q)$ , where  $-\frac{1}{2} < q \leq 0$ . A similar comment can be made for the boundary layer expansion (2.7) near  $x = 1$ . This observation is used in §3 and §4 to help evaluate certain integrals asymptotically.

A composite expansion for this equilibrium solution, valid for  $x \in [0, 1]$ , is obtained by combining (2.2) and (2.7). This yields,

$$u \sim \tilde{u}^\varepsilon[x; x_0] \equiv x - x_0 + u_{l_0}[\varepsilon^{-1}x; x_0] + u_{r_0}[\varepsilon^{-1}(1 - x); x_0] + \dots, \quad (2.12)$$

Here  $u_{l_0}$  and  $u_{r_0}$  satisfy (2.3) and (2.8), respectively. In (2.12), we have emphasized the parametric dependence of  $u_{l_0}$ ,  $u_{r_0}$  and  $\tilde{u}^\varepsilon$  on the unknown constant  $x_0$ , which satisfies  $0 < x_0 < 1$ . When  $f(u) = u^2/2$ , this constant represents the tip of the equilibrium parabolic-shaped flame-front interface. The difficulty in analytically determining the correct value for  $x_0$  still persists even after calculating higher order boundary layer corrections near each endpoint. By symmetry, when  $f(u)$  is even, the correct value is clearly  $x_0 = 1/2$ . However, to determine  $x_0$  analytically for general  $f(u)$  we must retain exponentially small terms in the asymptotic expansion of the solution. One way to do this is to use the projection method developed in [14] and [15].

## 2.1 The Projection Method

We now outline how this method can be used to determine the equilibrium value for  $x_0$  in (2.12) and to analyze metastability for the time-dependent problem (1.7). To analyze metastable behavior for (1.7), we seek a solution to (1.7) for  $t \gg 1$  in the form

$$u(x, t) = \tilde{u}^\varepsilon[x; x_0(t)] + v(x, t), \quad (2.13)$$

where  $v \ll \tilde{u}^\varepsilon$  and  $v_t \ll \partial_t \tilde{u}^\varepsilon$ . Linearizing (1.7) around  $\tilde{u}^\varepsilon$ , we obtain that  $v$  satisfies the quasi-steady problem

$$L_\varepsilon v = -R + x'_0 \partial_{x_0} \tilde{u}^\varepsilon, \quad 0 < x < 1, \quad (2.14a)$$

$$v(0, t) = -\tilde{u}^\varepsilon(0; x_0), \quad v(1, t) = -\tilde{u}^\varepsilon(1; x_0). \quad (2.14b)$$

Here the operator  $L_\varepsilon v$  and the residual  $R = R(x; x_0)$  are defined by

$$L_\varepsilon v \equiv \varepsilon v_{xx} - [f'(\tilde{u}^\varepsilon)v]_x + v f''(\tilde{u}^\varepsilon), \quad (2.15a)$$

$$R \equiv \varepsilon \tilde{u}^\varepsilon_{xx} - f'(\tilde{u}^\varepsilon) \tilde{u}^\varepsilon_x + f'(\tilde{u}^\varepsilon). \quad (2.15b)$$

Now let  $x_0$  be fixed and let  $\lambda_j, \phi_j$  for  $j \geq 0$  be the normalized eigenpairs of the associated eigenvalue problem

$$L_\varepsilon \phi = \lambda \phi, \quad 0 < x < 1; \quad \phi(0) = \phi(1) = 0. \quad (2.16)$$

The  $\lambda_j$  are real and the  $\phi_j$  satisfy the orthogonality relations

$$(\phi_j, \phi_k)_\omega = \delta_{jk}, \quad j, k = 0, 1, \dots \quad (2.17)$$

Here the inner product is defined by  $(u, v)_\omega \equiv \int_0^1 uv\omega dx$ , where the weight function  $\omega = \omega(x)$  is given by

$$\omega(x) \equiv \exp \left( -\varepsilon^{-1} \int_{x_0}^x f' [\tilde{u}^\varepsilon(z; x_0)] dz \right). \quad (2.18)$$

Upon integrating by parts, we obtain Lagrange's identity for any two smooth functions  $v$  and  $\phi$ ,

$$(\phi, L_\varepsilon v)_\omega = (\varepsilon \phi \omega v_x - \varepsilon \phi_x \omega v) \Big|_0^1 + (L_\varepsilon \phi, v)_\omega. \quad (2.19)$$

Next, we expand the solution  $v$  to (2.14) in terms of the eigenfunctions  $\phi_j$  as

$$v = \sum_{j=0}^{\infty} \frac{c_j}{\lambda_j} \phi_j. \quad (2.20)$$

The coefficients  $c_j$ , obtained from (2.14) and (2.19) are

$$c_j = -\varepsilon \phi_{jx} \omega \tilde{u}^\varepsilon \Big|_0^1 - (R, \phi_j)_\omega + x'_0 (\partial_{x_0} \tilde{u}^\varepsilon, \phi_j)_\omega. \quad (2.21)$$

As shown in §3, the severe indeterminacy in selecting the correct  $x_0$  for the equilibrium problem results in an exponentially small principal eigenvalue for (2.16). Since  $L_\varepsilon[\partial_{x_0} \tilde{u}^\varepsilon]$  is uniformly small on  $[0, 1]$  and  $\partial_{x_0} \tilde{u}^\varepsilon$  is of one sign, this suggests that  $\phi_0$  is proportional to  $\partial_{x_0} \tilde{u}^\varepsilon$ . Since  $\lambda_0 \rightarrow 0$  as  $\varepsilon \rightarrow 0$ , a necessary condition for the solvability of (2.14) is that  $c_0 \rightarrow 0$  as  $\varepsilon \rightarrow 0$ . Setting  $c_0 = 0$  in (2.21) we obtain an asymptotic differential equation for  $x_0 = x_0(t)$ :

$$x'_0 (\phi_0, \partial_{x_0} \tilde{u}^\varepsilon)_\omega = (R, \phi_0)_\omega + \varepsilon \phi_{0x} \omega \tilde{u}^\varepsilon \Big|_0^1. \quad (2.22)$$

The metastable dynamics for (1.7) is then characterized by  $u(x, t) \sim \tilde{u}^\varepsilon[x; x_0(t)]$ , where  $\tilde{u}^\varepsilon$  is defined in (2.12). The equilibrium value for  $x_0$ , corresponding to the equilibrium solution for  $u$ , is obtained by setting  $x'_0 = 0$  in (2.22), which yields the algebraic condition

$$(R, \phi_0)_\omega = -\varepsilon \phi_{0x} \omega \tilde{u}^\varepsilon \Big|_0^1. \quad (2.23)$$

This completes the outline of the projection method. In §3 we estimate  $\phi_0$  and  $\lambda_0$  as  $\varepsilon \rightarrow 0$ , and in §4 we evaluate the inner products in (2.22) and (2.23) asymptotically. These calculations allow us to explicitly determine the equilibrium value for  $x_0$  from (2.23) and the form of the ODE for  $x_0(t)$  in (2.22).

### 3 Asymptotics and Numerics for the Principal Eigenpair

We now estimate the principal eigenpair  $\lambda_0, \phi_0$  for (2.16). Let  $\tilde{\phi}_0$  be a comparison function for  $\phi_0$ . Then, from Lagrange's identity (2.19), we get

$$\lambda_0 \left( \tilde{\phi}_0, \phi_0 \right)_\omega = \left( L_\varepsilon \tilde{\phi}_0, \phi_0 \right)_\omega + \varepsilon \phi_{0x} \omega \tilde{\phi}_0 \Big|_0^1. \quad (3.1)$$

To get a very rough estimate for  $\lambda_0$  take  $\tilde{\phi}_0 = 1$  for which  $L_\varepsilon 1$  is exponentially small for  $O(\varepsilon) \ll x \ll 1 - O(\varepsilon)$ . Then, substituting  $\phi_0 \sim \partial_{x_0} \tilde{u}^\varepsilon$  into (3.1), and using the fact that  $\omega$  is exponentially small unless  $|x - x_0| = O(\varepsilon)$ , it is readily clear that  $\lambda_0 = O(e^{-c/\varepsilon})$  for some  $c > 0$ .

To get a precise estimate for  $\lambda_0$ , we first replace (2.16) with the approximate equation  $L_\varepsilon \phi_0 = 0$ . Then, in §3.1, we use boundary layer theory to construct  $\phi_0$  for  $\varepsilon \rightarrow 0$ . The outer solution for  $\phi_0$  is clearly  $\phi_0 \sim 1$  (apart from a normalization constant). In §3.2 we use (3.1) to estimate  $\lambda_0$ , and in §3.3 we compute  $\lambda_0$  numerically.

#### 3.1 Asymptotics for Principal Eigenfunction

In the left boundary layer we let  $y = \varepsilon^{-1}x$ ,  $\phi_l(y) = \phi_0(\varepsilon y)$ , and we expand  $\phi_l$  as

$$\phi_l(y) = 1 + \phi_{l_0}(y) + \varepsilon \phi_{l_1}(y) + \dots. \quad (3.2)$$

Substituting (3.2) into  $L_\varepsilon \phi_0 = 0$ , and using (2.2), we obtain that  $\phi_{l_0}$  satisfies

$$\phi_{l_0}'' - [f'(-x_0 + u_{l_0})(1 + \phi_{l_0})]' = 0, \quad 0 < y < \infty; \quad \phi_{l_0}(0) = -1, \quad \phi_{l_0}(\infty) = 0. \quad (3.3)$$

Comparing (3.3) with (2.3), we conclude that  $\phi_{l_0} = -\partial_{x_0} u_{l_0}$ . Therefore, we have

$$\phi_{l_0}'(0) = -f'(-x_0), \quad \phi_{l_0}(y) \sim (a_{l_0} \nu_l' y - a_{l_0}') e^{-\nu_l y}, \quad \text{as } y \rightarrow \infty. \quad (3.4)$$

At the next order, it is easily shown that  $\phi_{l_1} = -\partial_{x_0} u_{l_1}$ .

Similarly, in the right boundary layer we let  $y = \varepsilon^{-1}(1 - x)$ ,  $\phi_r(y) = \phi_0(1 - \varepsilon y)$ , and we expand  $\phi_r$  as

$$\phi_r(y) = 1 + \phi_{r_0}(y) + \varepsilon \phi_{r_1}(y) + \dots. \quad (3.5)$$

Substituting (3.5) and (2.7) into  $L_\varepsilon \phi_0 = 0$ , we get to leading order

$$\phi_{r_0}'' + [f'(1 - x_0 + u_{r_0})(1 + \phi_{r_0})]' = 0, \quad 0 < y < \infty; \quad \phi_{r_0}(0) = -1, \quad \phi_{r_0}(\infty) = 0. \quad (3.6)$$

Comparing (3.3) with (2.8), we have  $\phi_{r_0} = -\partial_{x_0} u_{r_0}$  and, hence,

$$\phi_{r_0}'(0) = f'(1 - x_0), \quad \phi_{r_0}(y) \sim (-a_{r_0} \nu_r' y + a_{r_0}') e^{-\nu_r y}, \quad \text{as } y \rightarrow \infty. \quad (3.7)$$

In addition, we have  $\phi_{r_1} = -\partial_{x_0} u_{r_1}$ . In the notation in (3.4), (3.7) and in the formulae to be derived below, the primes on the constants  $a_{l_0}, a_{r_0}, \nu_l$  and  $\nu_r$  denote derivatives with respect to  $x_0$ .

For similar reasons as outlined following (2.11) above, the expansions (3.2) and (3.5) hold only on the interval  $y = O(\varepsilon^q)$ , where  $-1/2 < q \leq 0$ . A composite expansion for  $\phi_0$ , valid for  $x \in [0, 1]$ , is

$$\phi_0(x) = 1 + \phi_{l_0}(\varepsilon^{-1}x) + \phi_{r_0}[\varepsilon^{-1}(1-x)] + \dots \quad (3.8)$$

This asymptotic eigenfunction can then be suitably normalized.

In the derivation below to estimate  $\lambda_0$  we require certain formulae involving the ratios  $\phi'_{r_0}/u'_{r_0}$  and  $\phi'_{l_0}/u'_{l_0}$ . The first identity is obtained by combining (2.3) and (3.3) to get

$$\frac{d}{dy} \left( \frac{\phi'_{l_0}}{u'_{l_0}} \right) = f''(-x_0 + u_{l_0}) (\phi_{l_0} + 1), \quad 0 < y < \infty, \quad (3.9a)$$

$$\frac{\phi'_{l_0}(0)}{u'_{l_0}(0)} = \frac{f'(-x_0)}{f(-x_0)}, \quad \frac{\phi'_{l_0}(y)}{u'_{l_0}(y)} = \nu'_l y - \frac{(a_{l_0} \nu_l)'}{a_{l_0} \nu_l} + o(1), \quad \text{as } y \rightarrow \infty. \quad (3.9b)$$

In a similar way, combining (2.8) and (3.6) we obtain

$$\frac{d}{dy} \left( \frac{\phi'_{r_0}}{u'_{r_0}} \right) = -f''(1 - x_0 + u_{r_0}) (\phi_{r_0} + 1), \quad 0 < y < \infty, \quad (3.10a)$$

$$\frac{\phi'_{r_0}(0)}{u'_{r_0}(0)} = \frac{f'(1 - x_0)}{f(1 - x_0)}, \quad \frac{\phi'_{r_0}(y)}{u'_{r_0}(y)} = \nu'_r y - \frac{(a_{r_0} \nu_r)'}{a_{r_0} \nu_r} + o(1), \quad \text{as } y \rightarrow \infty. \quad (3.10b)$$

## 3.2 Asymptotics for the Principal Eigenvalue

To estimate  $\lambda_0$  from (3.1) we choose the comparison function  $\tilde{\phi}_0 = 1$  and use (2.12) and (3.8) for  $\tilde{u}^\varepsilon$  and  $\phi_0$ , respectively. Substituting (3.8) and  $\tilde{\phi}_0 = 1$  into (3.1) we get

$$\lambda_0(1, \phi_0)_\omega \sim (L_\varepsilon 1, 1)_\omega + (L_\varepsilon 1, \phi_{l_0})_\omega + (L_\varepsilon 1, \phi_{r_0})_\omega - \phi'_{r_0}(0)\omega(1) - \phi'_{l_0}(0)\omega(0), \quad (3.11)$$

where  $(u, v)_\omega \equiv \int_0^1 u v \omega dx$  and  $\omega = \omega(x)$  is defined in (2.18). From (2.15a), we calculate

$$L_\varepsilon 1 = f''(\tilde{u}^\varepsilon)(1 - \tilde{u}_x^\varepsilon). \quad (3.12)$$

To evaluate the three integrals on the right side of (3.11) we break the range of integration for each integral into the three regions  $x \in [0, \varepsilon^p]$ ,  $x \in [\varepsilon^p, 1 - \varepsilon^p]$ , and  $x \in [1 - \varepsilon^p, 1]$ . Here the choice  $1/2 < p < 1$  gives an intermediate scaling between the outer and boundary layer regions and is needed to ensure that the leading order terms in the expansions for  $\phi_0$  and  $\tilde{u}^\varepsilon$  in the boundary layer regions are asymptotically valid (see the remark following (2.11) above). To determine which integrals are asymptotically dominant we make the following observations:  $\omega = O(1)$  for  $|x - x_0| = O(\varepsilon)$ ;  $\omega = \text{t.s.t.}$  for  $|x - x_0| \gg O(\varepsilon)$ ;  $\phi_{l_0} = \text{t.s.t.}$  for  $x \gg O(\varepsilon^p)$ ;  $\phi_{r_0} = \text{t.s.t.}$  for  $1 - x \gg O(\varepsilon^p)$ . From these considerations, we can reduce (3.11) asymptotically to

$$\lambda_0(1, 1)_\omega \sim (I_1 - \phi'_{l_0}(0)\omega(0)) + (I_2 - \phi'_{r_0}(0)\omega(1)) + I_3, \quad (3.13)$$

where

$$I_1 \equiv \int_0^{\varepsilon^p} \omega(1 + \phi_{l_0}) L_\varepsilon 1 dx, \quad I_2 \equiv \int_{1-\varepsilon^p}^1 \omega(1 + \phi_{r_0}) L_\varepsilon 1 dx, \quad I_3 \equiv \int_{\varepsilon^p}^{1-\varepsilon^p} \omega L_\varepsilon 1 dx. \quad (3.14)$$

We first estimate  $I_1$ . Letting  $y = \varepsilon^{-1}x$  and using (2.12) and (3.12) we get

$$I_1 \sim - \int_0^{\varepsilon^{p-1}} \omega u'_{l_0}(y) f''[-x_0 + u_{l_0}(y)] (1 + \phi_{l_0}(y)) dy. \quad (3.15)$$

As shown in (0.5) of Appendix A,  $\omega u'_{l_0}$  is asymptotically constant on  $[0, \varepsilon^{p-1}]$ . Then, substituting (3.9a) into (3.15) we get

$$I_1 \sim -\omega(0) u'_{l_0}(0) \int_0^{\varepsilon^{p-1}} \frac{d}{dy} \left( \frac{\phi'_{l_0}}{u'_{l_0}} \right) dy \sim -\omega(0) u'_{l_0}(0) \left( \frac{\phi'_{l_0}}{u'_{l_0}} \right) \Big|_0^{\varepsilon^{p-1}}. \quad (3.16)$$

Therefore, using (3.9b), we obtain

$$I_1 - \phi'_{l_0}(0) \omega(0) \sim -\omega(0) u'_{l_0}(0) \left[ \nu'_l \varepsilon^{p-1} - \frac{(a_{l_0} \nu_l)'}{a_{l_0} \nu_l} \right]. \quad (3.17)$$

The integral  $I_2$  can be estimated in a similar way by using (0.7) of Appendix A and (3.10) to derive

$$I_2 - \phi'_{r_0}(0) \omega(1) \sim -\omega(1) u'_{r_0}(0) \left[ \nu'_r \varepsilon^{p-1} - \frac{(a_{r_0} \nu_r)'}{a_{r_0} \nu_r} \right]. \quad (3.18)$$

Asymptotic formulae for  $\omega(0) u'_{l_0}(0)$  and  $\omega(1) u'_{r_0}(0)$  are given in (0.6) and (0.7) of Appendix A, respectively.

Next we estimate  $I_3$ . Using (3.12) and (2.12) we can decompose  $I_3$  as

$$I_3 \sim I_{3L} + I_{3R}; \quad I_{3L} \equiv - \int_{\varepsilon^p}^{1-\varepsilon^p} \omega f''(\tilde{u}^\varepsilon) u_{l_0x} dx, \quad I_{3R} \equiv - \int_{\varepsilon^p}^{1-\varepsilon^p} \omega f''(\tilde{u}^\varepsilon) u_{r_0x} dx. \quad (3.19)$$

For  $x \in [\varepsilon^p, 1 - \varepsilon^p]$  we have from (0.1) of Appendix A that  $\omega(x) = \exp[-f(x - x_0)/\varepsilon](1 + \text{t.s.t.})$ . Thus, using the decay behavior (2.3b) for  $u_{l_0}$  and  $\tilde{u}^\varepsilon \sim x - x_0$ ,  $I_{3L}$  becomes

$$I_{3L} \sim \varepsilon^{-1} a_{l_0} \nu_l \int_{\varepsilon^p}^{1-\varepsilon^p} f''(x - x_0) e^{-h_l(x)/\varepsilon} dx, \quad h_l(x) \equiv \nu_l x + f(x - x_0), \quad (3.20)$$

where  $\nu_l = -f'(-x_0)$ . Clearly  $h_l(x)$  has a minimum on  $[\varepsilon^p, 1 - \varepsilon^p]$  at  $x = \varepsilon^p$ . Thus, for  $\varepsilon \rightarrow 0$ , the dominant contribution to  $I_{3L}$  arises from the region near  $x = \varepsilon^p$ . Let  $x = \varepsilon^p + s$  in  $I_{3L}$  and expand  $h_l(x)$  and  $f''(x - x_0)$  near  $x = \varepsilon^p$  to get

$$I_{3L} \sim \varepsilon^{-1} a_{l_0} \nu_l e^{-f(-x_0)/\varepsilon} \int_0^\infty [f''(-x_0) + s f'''(-x_0) + \dots] \exp \left[ -\frac{1}{2\varepsilon} f''(-x_0) (s^2 + 2\varepsilon^p s + \varepsilon^{2p}) \right] ds. \quad (3.21)$$

Then, using Laplace's method and the bound  $1/2 < p < 1$ , we obtain as  $\varepsilon \rightarrow 0$

$$I_{3L} \sim a_{l_0} \nu_l e^{-f(-x_0)/\varepsilon} \left[ \left( \frac{\pi}{2\varepsilon} \right)^{1/2} [f''(-x_0)]^{1/2} - \varepsilon^{p-1} f''(-x_0) + \frac{f'''(-x_0)}{f''(-x_0)} \right]. \quad (3.22)$$

A similar calculation, which we shall omit, can be used to calculate  $I_{3R}$  as  $\varepsilon \rightarrow 0$ . We find,

$$I_{3R} \sim a_{r_0} \nu_r e^{-f(1-x_0)/\varepsilon} \left[ \left( \frac{\pi}{2\varepsilon} \right)^{1/2} [f''(1-x_0)]^{1/2} - \varepsilon^{p-1} f''(1-x_0) - \frac{f'''(1-x_0)}{f''(1-x_0)} \right]. \quad (3.23)$$

Finally, we estimate  $(1, 1)_\omega$  in (3.13). The dominant contribution to this integral arises from the region near  $x = x_0$ . Assuming that  $f''(0) > 0$ , we obtain upon using (0.1) of Appendix A and Laplace's method that

$$(1, 1)_\omega \sim \int_{-\infty}^{\infty} e^{-f(x-x_0)/\varepsilon} dx \sim \varepsilon^{1/2} \theta_0 (1 + \varepsilon \theta_1 + \dots), \quad (3.24a)$$

$$\theta_0 = \left( \frac{2\pi}{f''(0)} \right)^{1/2}, \quad \theta_1 = \left( -\frac{f'''(0)}{8[f''(0)]^2} + \frac{5[f'''(0)]^2}{24[f''(0)]^3} \right). \quad (3.24b)$$

To obtain our asymptotic estimate for  $\lambda_0$  we substitute (3.17), (3.18), (3.19), (3.22), (3.23) and (3.24) into (3.13). This leads to the following result:

**Proposition 1** *Let  $f(u)$  be smooth, convex, and satisfy  $f(0) = f'(0) = 0$  with  $f''(0) > 0$ . Then, for  $\varepsilon \rightarrow 0$  and  $0 < x_0 < 1$ , the principal eigenvalue  $\lambda_0$  for (2.16) satisfies*

$$\lambda_0 \sim \frac{[f''(0)]^{1/2}}{2\varepsilon} \left( a_{l_0} \nu_l e^{-f(-x_0)/\varepsilon} [b_{l_0} + \varepsilon^{1/2} b_{l_1} + \dots] + a_{r_0} \nu_r e^{-f(1-x_0)/\varepsilon} [b_{r_0} + \varepsilon^{1/2} b_{r_1} + \dots] \right), \quad (3.25)$$

where

$$b_{l_0} = [f''(-x_0)]^{1/2}, \quad b_{l_1} = \left( \frac{2}{\pi} \right)^{1/2} \left[ \frac{f'''(-x_0)}{f''(-x_0)} - \frac{(a_{l_0} \nu_l)'}{a_{l_0} \nu_l} \right], \quad (3.26a)$$

$$b_{r_0} = [f''(1-x_0)]^{1/2}, \quad b_{r_1} = -\left( \frac{2}{\pi} \right)^{1/2} \left[ \frac{f'''(1-x_0)}{f''(1-x_0)} - \frac{(a_{r_0} \nu_r)'}{a_{r_0} \nu_r} \right]. \quad (3.26b)$$

Here  $a_{l_0}$ ,  $\nu_l$ ,  $a_{r_0}$ , and  $\nu_r$ , which depend on  $x_0$ , are defined in (2.5) and (2.10). The primes on these coefficients indicate differentiation with respect to  $x_0$ .

This estimate for  $\lambda_0$  characterizes the ill-conditioning of the equilibrium problem (2.1). Since  $\lambda_0 > 0$  it also indicates that the equilibrium solution is marginally unstable.

### 3.3 Numerics for the Principal Eigenvalue

We now verify (3.25) by comparing it with full numerical results for  $\lambda_0$  computed from (2.16) for two choices of  $f(u)$  and for various values of  $x_0$  and  $\varepsilon$ . Numerical methods to compute eigenvalues include the software package SLEIGN and the NAG library code D02KDF (cf. [3], [7], [9]). Our approach to compute  $\lambda_0$  is to use the boundary value ODE solver COLSYS [1] with a suitable initial guess.

To numerically evaluate the operator  $L_\varepsilon$  in (2.16) we must first determine  $\tilde{u}^\varepsilon$  given in (2.12). In general, this requires us to numerically compute the boundary layer functions  $u_{l_0}$  and  $u_{r_0}$  satisfying (2.3) and (2.8) using COLSYS. Then, to compute  $\lambda_0$  we re-write (2.16) as a first order system. Using  $\lambda_0 = 0$  and (3.8) for  $\phi_0$  as initial guesses, we found that COLSYS readily converged to the principal eigenvalue for (2.16).

**Example 1:** Let  $f(u) = u^2/2$ , which corresponds to the flame-front problem (1.2). For this problem, we calculate from (2.5) and (2.10) that  $a_{l_0} = 2x_0$ ,  $\nu_l = x_0$ ,  $a_{r_0} = 2(1-x_0)$ , and  $\nu_r = 1-x_0$ . Thus, (3.25) becomes

$$\lambda_0 \sim \varepsilon^{-1} \left( x_0 \left[ x_0 - \left( \frac{8\varepsilon}{\pi} \right)^{1/2} \right] e^{-x_0^2/2\varepsilon} + (1-x_0) \left[ (1-x_0) - \left( \frac{8\varepsilon}{\pi} \right)^{1/2} \right] e^{-(1-x_0)^2/2\varepsilon} \right). \quad (3.27)$$

For this example,  $u_{l_0}(y; x_0)$  and  $u_{r_0}(y; x_0)$  can be found analytically as

$$u_{l_0}(y) = x_0 - x_0 \tanh\left(\frac{x_0 y}{2}\right), \quad u_{r_0}(y) = (1-x_0) \left[ \tanh\left(\frac{(1-x_0)y}{2}\right) - 1 \right]. \quad (3.28)$$

Thus, the composite expansion  $\tilde{u}^\varepsilon$ , which is needed in (2.16), is obtained explicitly.

**Example 2:** Here we choose the function  $f(u) = u - 2 + 4/(u+2)$ , which is not even. A careful calculation from (2.5) and (2.10) yields

$$\nu_l = -1 + \frac{4}{(2-x_0)^2} \quad a_{l_0} = x_0 \exp \left[ 4(2-x_0)^{-2} \log \left( \frac{4-x_0}{2} \right) \right], \quad (3.29a)$$

$$\nu_r = 1 - \frac{4}{(3-x_0)^2} \quad a_{r_0} = (1-x_0) \exp \left[ 4(3-x_0)^{-2} \log \left( \frac{5-x_0}{2} \right) \right]. \quad (3.29b)$$

Substituting (3.29) into (3.25) gives the asymptotic result for  $\lambda_0$ . For this example the boundary layer functions, and hence  $L_\varepsilon$ , must be computed numerically.

In Table 1–4 we display the asymptotic and numerical results for  $\lambda_0$  for each of the two examples. In each of these tables, the second column gives the numerical results for  $\lambda_0$ , while the third and fifth columns show the asymptotic expansion (3.25) with one term and two terms in the pre-exponential factors, respectively. In the fourth and sixth columns we display the relative error

$$\text{rate} = \frac{\lambda_0(\text{asy.}) - \lambda_0(\text{num.})}{\lambda_0(\text{num.})}. \quad (3.30)$$

Here  $\lambda_0(\text{asy.})$  denotes the asymptotic result with either one or two terms in the pre-exponential factors.

$\varepsilon$	$\lambda_0$ (num.)	$\lambda_0$ (3.27) 1-term	rate1	$\lambda_0$ (3.27) 2-term	rate2
0.004	$0.2676 \times 10^{-11}$	$0.3351 \times 10^{-11}$	0.252	$0.2674 \times 10^{-11}$	$-6.13 \times 10^{-4}$
0.006	$0.5626 \times 10^{-7}$	$0.7465 \times 10^{-7}$	0.327	$0.5619 \times 10^{-7}$	$-1.23 \times 10^{-3}$
0.008	$0.7333 \times 10^{-5}$	$0.1023 \times 10^{-4}$	0.395	$0.7312 \times 10^{-5}$	$-2.88 \times 10^{-3}$
0.010	$0.1276 \times 10^{-3}$	$0.1863 \times 10^{-3}$	0.461	$0.1269 \times 10^{-3}$	$-5.57 \times 10^{-3}$
0.012	$0.8182 \times 10^{-3}$	$0.1247 \times 10^{-2}$	0.524	$0.8111 \times 10^{-3}$	$-8.70 \times 10^{-3}$

Table 1: Example 1: Comparison of asymptotic and numerical values for  $\lambda_0$  with  $f(u) = u^2/2$  and  $x_0 = 0.50$ .

$\varepsilon$	$\lambda_0$ (num.)	$\lambda_0$ (3.27) 1-term	rate1	$\lambda_0$ (3.27) 2-term	rate2
0.002	$0.2443 \times 10^{-11}$	$0.3068 \times 10^{-11}$	0.256	$0.2442 \times 10^{-11}$	$-3.52 \times 10^{-4}$
0.003	$0.4168 \times 10^{-7}$	$0.5548 \times 10^{-7}$	0.331	$0.4163 \times 10^{-7}$	$-1.31 \times 10^{-3}$
0.004	$0.4893 \times 10^{-5}$	$0.6854 \times 10^{-5}$	0.401	$0.4878 \times 10^{-5}$	$-3.08 \times 10^{-3}$
0.006	$0.4920 \times 10^{-3}$	$0.7526 \times 10^{-3}$	0.530	$0.4868 \times 10^{-3}$	$-1.05 \times 10^{-2}$
0.008	$0.4369 \times 10^{-2}$	$0.7244 \times 10^{-2}$	0.658	$0.4290 \times 10^{-2}$	$-1.81 \times 10^{-2}$
0.010	$0.1476 \times 10^{-1}$	$0.2680 \times 10^{-1}$	0.815	$0.1458 \times 10^{-1}$	$-1.22 \times 10^{-2}$

Table 2: Example 1: Comparison of asymptotic and numerical values for  $\lambda_0$  with  $f(u) = u^2/2$  and  $x_0 = 0.35$ .

From these tables we observe that a two-term asymptotic expansion for the pre-exponential factor of  $\lambda_0$  is certainly needed to obtain close quantitative agreement with the numerical results for  $\lambda_0$ . A similar situation was found in [11] for some related problems with exponentially small eigenvalues. From Tables 1 and 2 we find that, in most cases, the relative errors for the two-term expansion in most cases are below 1 %, while they are only between 20 % and 70 % for the one-term expansion. Similar behavior is observed in Tables 3 and 4 for the relative errors for Example 2.

## 4 Derivation of the Metastable Dynamics

We now asymptotically evaluate the various terms in (2.22) to obtain an explicit ODE for  $x_0 = x_0(t)$ . The metastable dynamics for (1.7) is then given by  $u(x, t) \sim \tilde{u}^\varepsilon[x; x_0(t)]$ , where  $\tilde{u}^\varepsilon$  is defined in (2.12).

Similar considerations as given following (3.12) above show that (2.22) reduces asymptotically to

$$-x_0'(1, 1)_\omega \sim I_1 + I_2 + I_3, \quad (4.1)$$

$\varepsilon$	$\lambda_0$ (num.)	$\lambda_0$ (3.25) 1-term	rate1	$\lambda_0$ (3.25) 2-term	rate2
0.00325	$0.3888 \times 10^{-11}$	$0.5267 \times 10^{-11}$	0.354	$0.3791 \times 10^{-11}$	$-2.49 \times 10^{-2}$
0.00350	$0.3210 \times 10^{-10}$	$0.4405 \times 10^{-10}$	0.372	$0.3124 \times 10^{-10}$	$-2.68 \times 10^{-2}$
0.00400	$0.9736 \times 10^{-9}$	$0.1371 \times 10^{-8}$	0.408	$0.9448 \times 10^{-8}$	$-2.96 \times 10^{-2}$
0.00450	$0.1358 \times 10^{-7}$	$0.1961 \times 10^{-7}$	0.444	$0.1314 \times 10^{-7}$	$-3.24 \times 10^{-2}$
0.00500	$0.1101 \times 10^{-6}$	$0.1629 \times 10^{-6}$	0.480	$0.1063 \times 10^{-6}$	$-3.45 \times 10^{-2}$
0.00550	$0.6026 \times 10^{-6}$	$0.9129 \times 10^{-6}$	0.515	$0.5798 \times 10^{-6}$	$-3.78 \times 10^{-2}$
0.00600	$0.2458 \times 10^{-5}$	$0.3809 \times 10^{-5}$	0.549	$0.2357 \times 10^{-5}$	$-4.11 \times 10^{-2}$

Table 3: Example 2: Comparison of asymptotic and numerical values for  $\lambda_0$  with  $f(u) = u - 2 + 4/(u + 2)$  and  $x_0 = 0.40$ .

$\varepsilon$	$\lambda_0$ (num.)	$\lambda_0$ (3.25) 1-term	rate1	$\lambda_0$ (3.25) 2-term	rate2
0.00225	$0.4172 \times 10^{-12}$	$0.5519 \times 10^{-12}$	0.323	$0.4082 \times 10^{-12}$	$-2.16 \times 10^{-2}$
0.00250	$0.9997 \times 10^{-11}$	$0.1346 \times 10^{-10}$	0.347	$0.9769 \times 10^{-11}$	$-2.28 \times 10^{-2}$
0.00300	$0.1137 \times 10^{-8}$	$0.1584 \times 10^{-8}$	0.393	$0.1107 \times 10^{-8}$	$-2.64 \times 10^{-2}$
0.00350	$0.3239 \times 10^{-7}$	$0.4659 \times 10^{-7}$	0.439	$0.3145 \times 10^{-7}$	$-2.90 \times 10^{-2}$
0.00425	$0.1077 \times 10^{-5}$	$0.1621 \times 10^{-5}$	0.506	$0.1041 \times 10^{-5}$	$-3.34 \times 10^{-2}$
0.00550	$0.4114 \times 10^{-4}$	$0.6645 \times 10^{-4}$	0.615	$0.3937 \times 10^{-4}$	$-4.30 \times 10^{-2}$
0.00650	$0.2637 \times 10^{-3}$	$0.4489 \times 10^{-3}$	0.702	$0.2500 \times 10^{-3}$	$-5.20 \times 10^{-2}$

Table 4: Example 2: Comparison of asymptotic and numerical values for  $\lambda_0$  with  $f(u) = u - 2 + 4/(u + 2)$  and  $x_0 = 0.35$ .

where the  $I_j$ , for  $j = 1, 2, 3$ , are defined by

$$I_1 \equiv \int_0^{\varepsilon^p} \omega(1 + \phi_{l_0})R dx, \quad I_2 \equiv \int_{1-\varepsilon^p}^1 \omega(1 + \phi_{r_0})R dx, \quad I_3 \equiv \int_{\varepsilon^p}^{1-\varepsilon^p} \omega R dx. \quad (4.2)$$

Here  $R$  is defined in (2.15b) and  $1/2 < p < 1$  gives the intermediate scaling used in §3. We note that the boundary term  $\varepsilon \phi_{0x} \omega \tilde{u}^\varepsilon \Big|_0^1$  in (2.22) can be neglected in comparison to each  $I_j$  since it involves the product of the two exponentially small terms  $\omega$  and  $\tilde{u}^\varepsilon$  at  $x = 0, 1$ . To calculate  $R$  we substitute (2.12) into (2.15b) and use (2.3a) and (2.8a) to get

$$R \sim [f'(-x_0 + u_{l_0}) - f'(\tilde{u}^\varepsilon)] u_{l_{0x}} + [f'(1 - x_0 + u_{r_0}) - f'(\tilde{u}^\varepsilon)] u_{r_{0x}}. \quad (4.3)$$

The inner product  $(1, 1)_\omega$  in (4.1) was calculated for  $\varepsilon \rightarrow 0$  in (3.24).

We first estimate  $I_1$ . In the region  $0 < x < \varepsilon^p$  we can approximate  $R$  by  $R \sim -f''(-x_0 + u_{l_0})x u_{l_{0x}}$ . Substituting this expression into  $I_1$  and letting  $y = \varepsilon^{-1}x$  we obtain, upon using (3.9a) and (0.5) of

Appendix A, that

$$I_1 \sim -\varepsilon \int_0^{\varepsilon^{p-1}} \omega u'_{l_0} y f''(-x_0 + u_{l_0}) (1 + \phi_{l_0}) dy \sim -\varepsilon \omega(0) u'_{l_0}(0) \int_0^{\varepsilon^{p-1}} y \frac{d}{dy} \left( \frac{\phi'_{l_0}}{u'_{l_0}} \right) dy. \quad (4.4)$$

Then, since  $\phi'_{l_0} = -\partial_{x_0} u'_{l_0}$  and  $u'_{l_0} < 0$  we can re-write (4.4) after integrating by parts as

$$I_1 \sim \varepsilon \omega(0) u'_{l_0}(0) \partial_{x_0} \left[ y \log(-u'_{l_0}) \Big|_0^{\varepsilon^{p-1}} - \int_0^{\varepsilon^{p-1}} \log(-u'_{l_0}) dy \right]. \quad (4.5)$$

Recall from (2.3b) that  $u'_{l_0} \sim -a_{l_0} \nu_l e^{-\nu_l y}$  as  $y \rightarrow \infty$ . Since  $\varepsilon^{p-1} \rightarrow \infty$  as  $\varepsilon \rightarrow 0$  for  $1/2 < p < 1$  we can use this decay behavior to estimate  $\log(-u'_{l_0})$  at the upper endpoint  $y = \varepsilon^{p-1}$ . In addition, we can add and subtract the term  $\log(a_{l_0} \nu_l) - \nu_l y$  inside the integrand in (4.5) so that the resulting integral converges when the upper limit of integration is set to infinity. In this way, we obtain that

$$I_1 \sim \varepsilon \omega(0) u'_{l_0}(0) \left( -\frac{\nu'_l}{2} \varepsilon^{2p-2} + \beta_l \right), \quad (4.6)$$

Here  $\nu'_l \equiv d\nu_l/dx_0 = f''(-x_0)$  from (2.5a), and  $\beta_l = \beta_l(x_0)$  is defined by

$$\beta_l \equiv -\frac{d}{dx_0} \left( \int_0^\infty [\log(-u'_{l_0}(y)) - \log(a_{l_0} \nu_l) + \nu_l y] dy \right). \quad (4.7)$$

A very similar calculation can be done to estimate  $I_2$  in (4.2). In the region  $1 - \varepsilon^p < x < 1$ , we have  $R \sim -f''(1 - x_0 + u_{r_0})(x - 1)u_{r_0x}$  in (4.2). Thus, upon using (0.7) of Appendix A and (3.10a),  $I_2$  becomes

$$I_2 \sim -\varepsilon \int_0^{\varepsilon^{p-1}} \omega u'_{r_0} y f''(1 - x_0 + u_{r_0}) (1 + \phi_{r_0}) dy \sim \varepsilon \omega(1) u'_{r_0}(0) \int_0^{\varepsilon^{p-1}} y \frac{d}{dy} \left( \frac{\phi'_{r_0}}{u'_{r_0}} \right) dy. \quad (4.8)$$

Then, since  $\phi'_{r_0} = -\partial_{x_0} u'_{r_0}$  and  $u'_{r_0} > 0$  we can re-write (4.8) after integrating by parts as

$$I_2 \sim -\varepsilon \omega(1) u'_{r_0}(0) \partial_{x_0} \left[ y \log(u'_{r_0}) \Big|_0^{\varepsilon^{p-1}} - \int_0^{\varepsilon^{p-1}} \log(u'_{r_0}) dy \right]. \quad (4.9)$$

Finally, using  $u'_{r_0} \sim a_{r_0} \nu_r e^{-\nu_r y}$  as  $y \rightarrow \infty$  in (4.9) we obtain, in analogy with (4.6), that

$$I_2 \sim -\varepsilon \omega(1) u'_{r_0}(0) \left( -\frac{\nu'_r}{2} \varepsilon^{2p-2} + \beta_r \right), \quad (4.10)$$

Here  $\nu'_r \equiv -f''(1 - x_0)$  and  $\beta_r$  is defined by

$$\beta_r \equiv -\frac{d}{dx_0} \left( \int_0^\infty [\log(u'_{r_0}(y)) - \log(a_{r_0} \nu_r) + \nu_r y] dy \right). \quad (4.11)$$

Next we estimate  $I_3$  in (4.2). Using (4.3) we first decompose  $I_3$  as  $I_3 \sim I_{3L} + I_{3R}$ , where

$$I_{3L} \sim \int_{\varepsilon^p}^{1-\varepsilon^p} \omega u_{l_0x} [f'(-x_0 + u_{l_0}) - f'(\tilde{u}^\varepsilon)] dx, \quad I_{3R} \sim \int_{\varepsilon^p}^{1-\varepsilon^p} \omega u_{r_0x} [f'(1 - x_0 + u_{r_0}) - f'(\tilde{u}^\varepsilon)] dx. \quad (4.12)$$

The dominant contribution to  $I_{3L}$  arises from the region near  $x = \varepsilon^p$ . To calculate  $I_{3L}$  we use (0.1) of Appendix A to estimate  $\omega$ , (2.3b) to evaluate  $u_{l_0x}$ , and we expand  $f'(-x_0 + u_{l_0}) - f'(\tilde{u}^\varepsilon)$  for  $x \rightarrow 0$ . This yields,

$$I_{3L} \sim \varepsilon^{-1} a_{l_0} \nu_l \int_{\varepsilon^p}^{1-\varepsilon^p} \left( x f''(-x_0) + \frac{x^2}{2} f'''(-x_0) + \dots \right) e^{-h_l(x)/\varepsilon} dx, \quad h_l(x) \equiv \nu_l x + f(x - x_0). \quad (4.13)$$

It is clear that  $h_l(x)$  is minimized on  $[\varepsilon^p, 1 - \varepsilon^p]$  at  $x = \varepsilon^p$ . Therefore, we can use Laplace's method to evaluate (4.13) by expanding  $h_l(x)$  as  $x \rightarrow 0$ . In this way, we obtain for  $\varepsilon \rightarrow 0$  that

$$I_{3L} \sim a_{l_0} \nu_l e^{-f(-x_0)/\varepsilon} \left( 1 - \frac{\varepsilon^{2p-1}}{2} f''(-x_0) + \dots \right). \quad (4.14)$$

A similar calculation, which we shall omit, can be done to calculate  $I_{3R}$  as  $\varepsilon \rightarrow 0$ , with the result

$$I_{3R} \sim -a_{r_0} \nu_r e^{-f(1-x_0)/\varepsilon} \left( 1 - \frac{\varepsilon^{2p-1}}{2} f''(1-x_0) + \dots \right). \quad (4.15)$$

Then,  $I_3$  in (4.2) is given by  $I_3 \sim I_{3L} + I_{3R}$ .

Finally, an explicit ODE for  $x_0 = x_0(t)$  is obtained by substituting (3.24), (4.6), (4.10), (4.14) and (4.15) into (4.1). The formulae (0.6) and (0.7) of Appendix A are used to evaluate  $\omega(0)u'_{l_0}(0)$  and  $\omega(1)u'_{r_0}(0)$ , respectively. This leads to our main result.

**Proposition 2 (Metastable Dynamics):** *Let  $f(u)$  be smooth, convex, and satisfy  $f(0) = f'(0) = 0$  with  $f''(0) > 0$ . Then, for  $\varepsilon \rightarrow 0$  and  $t \gg 1$ , the metastable dynamics for (1.7) is given by  $u(x, t) \sim \tilde{u}^\varepsilon[x; x_0(t)]$ , where  $\tilde{u}^\varepsilon$  is given in (2.12) and  $x_0(t)$  satisfies the asymptotic nonlinear ODE*

$$x'_0 \sim \varepsilon^{-1/2} \theta_0^{-1} (1 + \varepsilon \theta_1)^{-1} \left[ a_{r_0} \nu_r (1 + \varepsilon \beta_r) e^{-f(1-x_0)/\varepsilon} - a_{l_0} \nu_l (1 - \varepsilon \beta_l) e^{-f(-x_0)/\varepsilon} \right]. \quad (4.16)$$

The coefficients  $a_{l_0}$ ,  $\nu_l$ ,  $a_{r_0}$ ,  $\nu_r$ ,  $\beta_l$  and  $\beta_r$ , which all depend on  $x_0$ , are defined in (2.5), (2.10), (4.7) and (4.11). In addition,  $\theta_0$  and  $\theta_1$  are given in (3.24b).

The following equilibrium result is obtained by setting  $x'_0 = 0$  in (4.16):

**Corollary 1 (Equilibrium):** *The (unstable) equilibrium solution to (1.7) of the form given in (2.12) is  $u \sim \tilde{u}^\varepsilon[x; x_0^m]$ , where  $x_0^m$  satisfies the nonlinear algebraic equation*

$$a_{r_0} \nu_r (1 + \varepsilon \beta_r) e^{-f(1-x_0)/\varepsilon} \sim a_{l_0} \nu_l (1 - \varepsilon \beta_l) e^{-f(-x_0)/\varepsilon}. \quad (4.17)$$

The special case  $f(u) = u^2/2$  corresponds to the flame–front problem (1.1) (or equivalently (1.2)). For this special case,  $a_{l_0} = 2x_0$ ,  $\nu_l = x_0$ ,  $a_{r_0} = 2(1 - x_0)$  and  $\nu_r = 1 - x_0$ . In addition, since  $u_{l_0}$  and  $u_{r_0}$  are given analytically in (3.28), we can calculate  $\beta_l$  and  $\beta_r$  explicitly as

$$\beta_r = 2 \frac{d}{dx_0} \left( \int_0^\infty \log [1 + e^{-(1-x_0)y}] dy \right) = \frac{\pi^2}{6(1-x_0)^2}, \quad \beta_l = -\frac{\pi^2}{6x_0^2}. \quad (4.18)$$

In addition, when  $f(u) = u^2/2$ , we have  $\theta_0 = (2\pi)^{1/2}$  and  $\theta_1 = 0$ . Substituting these formulae into (4.16) yields the following explicit metastability result for (1.1) (or (1.2)):

**Corollary 2 (Metastable Flame–Front Dynamics):** *For  $\varepsilon \rightarrow 0$  and  $t \gg 1$ , the tip  $x_0 = x_0(t)$  of the metastable parabolic-shaped flame–front interface for (1.1) satisfies the asymptotic nonlinear ODE*

$$x'_0 \sim \sqrt{\frac{2}{\pi\varepsilon}} \left[ \left( (1-x_0)^2 + \frac{\pi^2\varepsilon}{3} \right) e^{-(1-x_0)^2/2\varepsilon} - \left( x_0^2 + \frac{\pi^2\varepsilon}{3} \right) e^{-x_0^2/2\varepsilon} \right]. \quad (4.19)$$

Some trends can be observed from these results. Let  $x_0^0 \equiv x_0(0)$  denote the initial condition for (4.16). Then, since for  $x_0^0 < x_0^m$  ( $x_0^0 > x_0^m$ ) we have  $x'_0 < 0$  ( $x'_0 > 0$ ) from (4.16), it follows that  $x_0(t)$  will not approach  $x_0^m$  as  $t \rightarrow \infty$ , but instead will eventually hit the wall at  $x = 0$  ( $x = 1$ ). In addition, when  $O(\varepsilon) \ll x_0 \ll 1 - O(\varepsilon)$ , (4.16) shows that  $x'_0$  is exponentially small and hence the motion is metastable. It is also clear that unless  $x_0^0$  is within an  $O(\varepsilon)$  neighborhood of  $x_0^m$  only one of the exponentials on the right side of (4.16) is significant for  $\varepsilon \rightarrow 0$ . Finally, in the case when  $f(u)$  is even, it is easy to see from the definitions of the coefficients in (4.17) that  $\beta_l = -\beta_r$ ,  $a_{l_0} = a_{r_0}$  and  $\nu_l = \nu_r$ . Hence, in this case we have  $x_0^m = 1/2$  as expected.

## 5 Comparison of Asymptotic and Numerical Results

We now compare the asymptotic results (4.16), (4.17) and (4.19) with corresponding full numerical results computed directly from (1.2), (1.7) and (2.1).

To compute numerical solutions to (1.7) we use a transverse method of lines approach (cf. [2]). This method is based on replacing the time derivative in (1.7) by a difference approximation and then solving the resulting boundary value problems in space. More specifically, suppose  $t_j$ , for  $j = 0, 1, \dots$ , are the grid points in time that are determined in the actual computation using a time–stepping control strategy. Then, we convert the time–dependent problem (1.7) to a set of boundary value problems using the Backward Differentiation Formulas (BDF) (cf. [2])

$$\sum_{j=0}^k \alpha_j u_{n-j}(x) = h_n N u_n(x), \quad u_n(0) = u_n(1) = 0. \quad (5.1)$$

Here  $\alpha_0 = 1$ ,  $h_j = t_j - t_{j-1}$ , and the differential operator  $N$  is defined by  $Nu = \varepsilon u''(x) - f'(u)u'(x) + f'(u)$ . The other coefficients  $\alpha_j$ , for  $j > 0$ , which depend only on  $h_j$ , for  $j = n, n-1, \dots, n-k+1$ , can be

computed numerically using Gaussian elimination in such a way that the BDF scheme (5.1) is  $k$ -th order accurate in time.

For every fixed  $n$ , (5.1) is a set of two-point boundary value problems with homogeneous boundary conditions that we solve at each time step using COLSYS ([1]). Although this approach is computationally expensive it yields approximate solutions to (1.7) that are highly accurate in space. As a result of the occurrence of the dramatic changes in time scales for (1.7), we found it necessary to implement a time-stepping control strategy to efficiently track the solution to (1.7) over long time intervals. To achieve this, we employed a higher (e. g. ,  $(k + 1)$ -th) order BDF scheme at each time step, and used the  $l_2$ -norm of the difference between the solutions of the  $k$ -th and the  $(k + 1)$ -th order BDF schemes as an error indicator to reject large inaccurate time steps or to enlarge unnecessary small time steps. In all of the calculation below we took  $k = 2$ .

The metastability results (4.16) and (4.19) are valid only after the completion of an  $O(1)$  transient period that describes the formation of the quasi-equilibrium solution (2.12) from initial data. As discussed in §1, a metastable quasi-equilibrium solution will not be formed for arbitrary initial data  $u_0(x)$ . A sufficient condition on  $u_0(x)$  for metastability to occur is given in (1.3). To eliminate the effect of the initial transient, in the computations below we took  $u(x, 0) = \tilde{u}^\varepsilon(x; x_0^0)$  as the initial data for (1.7) and (1.2). Here  $\tilde{u}^\varepsilon$  is the quasi-equilibrium profile given in (2.12) and  $x_0^0 \in (0, 1)$  is the initial zero of  $u$ . The value  $x_0^0$  is then used as the initial condition for the asymptotic ODE's (4.16) and (4.19) (i. e.  $x_0(0) = x_0^0$ ). With this initial condition, these ODE's are solved for  $t = t(x_0)$  using a numerical quadrature.

Asymptotic and numerical results for  $t = t(x_0)$  are compared for  $f(u) = u^2/2$  and for the asymmetric  $f(u)$  of Example 2 in §3.3 given by

$$f(u) = u - 2 + \frac{4}{u + 2}. \quad (5.2)$$

For this latter form of  $f(u)$ , explicit formulas for  $\nu_l$ ,  $a_{l_0}$ ,  $\nu_r$ , and  $a_{r_0}$  are given in (3.29). In this case, the functions  $\beta_l(x_0)$  and  $\beta_r(x_0)$  in (4.16) are calculated from a numerical quadrature after first using COLSYS to solve for the boundary layer functions  $u'_{l_0}$  and  $u'_{r_0}$ . For the  $f(u)$  of (5.2) we have  $\theta_0 = (2\pi)^{1/2}$  and  $\theta_1 = 3/32$  in (4.16).

For  $f(u) = u^2/2$ , in Table 5 and 6, we compare the asymptotic and numerical results for the tip  $t = t(x_0)$  of the flame-front interface for  $\varepsilon = 0.004$  and  $\varepsilon = 0.002$ , respectively. The initial tip location of the interface was  $x_0^0 = 0.4$  for  $\varepsilon = 0.004$  and  $x_0^0 = 0.3$  for  $\varepsilon = 0.002$ . The asymptotic and numerical results for the elapsed time agree to roughly within 2% for each of these examples. In Fig. 6 we plot, at different times, the numerical solution to (1.2) for  $\varepsilon = 0.002$  with the initial data  $u(x, 0) = \tilde{u}^\varepsilon(x; x_0^0)$ , where  $x_0^0 = 0.3$ . In Fig. 7 we compare the asymptotic and numerical tip trajectories  $t = t(x_0)$  for different initial conditions  $x_0^0$  when  $\varepsilon = 0.005$ . A logarithmic (base 10) scale is used for the vertical axis and the horizontal axis represents the parabolic tip location  $x_0$ . On this logarithmic scale, the asymptotic and numerical results are virtually indistinguishable.

For the asymmetric  $f(u)$  of (5.2), in Tables 7 and 8 we give a similar comparison between the asymptotic and numerical results for  $t = t(x_0)$  for  $\varepsilon = 0.004$  and  $\varepsilon = 0.003$ , respectively. The initial zeroes  $x_0^0$

$x_0$	t(num.)	t(asy.)
0.3999125	$0.196752251 \times 10^5$	$0.192198642 \times 10^5$
0.3972259	$0.554179455 \times 10^6$	$0.541388563 \times 10^6$
0.3943236	$0.997547019 \times 10^6$	$0.974550456 \times 10^6$
0.3829263	$0.197541881 \times 10^7$	$0.193020273 \times 10^7$
0.3636165	$0.235602159 \times 10^7$	$0.230237584 \times 10^7$
0.3094434	$0.245565007 \times 10^7$	$0.240006441 \times 10^7$
0.2514594	$0.245728124 \times 10^7$	$0.240171229 \times 10^7$
0.2005907	$0.245732411 \times 10^7$	$0.240176186 \times 10^7$
0.1122723	$0.245732918 \times 10^7$	$0.240176776 \times 10^7$

Table 5: A comparison of the asymptotic and numerical results for the tip  $t = t(x_0)$  of the flame-front for (1.2) with  $\varepsilon = 0.004$  and  $x_0^0 = 0.4$ .

of  $u$  are given in the tables. For both values of  $\varepsilon$ , the agreement between the asymptotic and numerical results is slightly closer than that for the case  $f(u) = u^2/2$ . For the  $f(u)$  in (5.2), in Fig. 8 we plot the numerical solution to (1.7) at different times when  $\varepsilon = 0.004$ . In Fig. 9 we compare some asymptotic and numerical trajectories for  $t = t(x_0)$  for different initial conditions  $x_0^0$  when  $\varepsilon = 0.006$ .

For the asymmetric  $f(u)$  of (5.2), we now verify the asymptotic result (4.17) for the equilibrium location  $x_0 = x_0^m$  corresponding to the equilibrium solution  $u \sim \tilde{u}^\varepsilon(x; x_0^m)$ . In Table 9 we compare asymptotic and numerical results for  $x_0^m$  at different values of  $\varepsilon$ . The asymptotic result for  $x_0^m$  was computed from (4.17) using Newton's method. The numerical value for  $x_0^m$  was computed from (2.1) using COLSYS (cf. [1]). As expected, the asymptotic results provide a closer determination of the corresponding numerical result as  $\varepsilon$  is decreased.

Finally, we show how to recover the solution  $y(x, t)$  to (1.1) from  $u(x, t)$ . Since  $u = -y_x$ , we have

$$y(x, t) = h(t) - \int_0^x u(s, t) ds, \quad (5.3)$$

where  $h(t)$  is to be found. To determine  $h(t)$ , we substitute (5.3) into (1.1a) to derive

$$h(t) = \int_0^t \left\{ -\varepsilon u_x(0) + \int_0^1 \int_0^x u(s, t) ds dx \right\} dt. \quad (5.4)$$

Since (1.1a) is invariant under a constant shift in  $y$ , we have taken  $h(0) = 0$ .

To determine  $h(t)$  during the metastable evolution we substitute  $u(x, t) \sim \tilde{u}^\varepsilon[x; x_0(t)]$  into (5.3) and (5.5). Here  $\tilde{u}^\varepsilon$  is given by (2.12), where  $u_{l_0}$  and  $u_{r_0}$  are given in (3.28). This yields,

$$y(x, t) = h(t) - \left\{ \frac{1}{2}x^2 - x_0x + 2\varepsilon \log 2 - 2\varepsilon \log(1 + e^{-x_0x/\varepsilon}) + 2\varepsilon \left[ \log(1 + e^{-(1-x_0)/\varepsilon}) - \log(1 + e^{-(1-x_0)(1-x)/\varepsilon}) \right] \right\}, \quad (5.5a)$$

$x_0$	t(num.)	t(asy.)
0.2996765	$0.110811891 \times 10^7$	$0.108295000 \times 10^7$
0.2958542	$0.109730472 \times 10^8$	$0.107247855 \times 10^8$
0.2907243	$0.180669282 \times 10^8$	$0.176594370 \times 10^8$
0.2875337	$0.205054498 \times 10^8$	$0.200430705 \times 10^8$
0.2704028	$0.245669157 \times 10^8$	$0.240128133 \times 10^8$
0.2500379	$0.250251570 \times 10^8$	$0.244610251 \times 10^8$
0.2306506	$0.250644804 \times 10^8$	$0.244996311 \times 10^8$
0.1811032	$0.250699164 \times 10^8$	$0.245050448 \times 10^8$
0.0903085	$0.250699778 \times 10^8$	$0.245051150 \times 10^8$

Table 6: A comparison of the asymptotic and numerical results for the tip  $t = t(x_0)$  of the flame-front for (1.2) with  $\varepsilon = 0.002$  and  $x_0^0 = 0.3$ .

where  $h(t)$  is defined by

$$\begin{aligned}
h(t) &= \int_0^t \left\{ -\frac{\pi^2 \varepsilon^2}{6x_0(1-x_0)} + \varepsilon(\log 4 - 1) + \frac{1}{2}x_0^2 - \frac{1}{2}x_0 + \frac{1}{6} + 2\varepsilon \log(1 + e^{-(1-x_0)/\varepsilon}) \right. \\
&\quad \left. + \frac{1}{2}(1-x_0)^2 \left[ 1 - \tanh^2 \frac{1-x_0}{2\varepsilon} \right] - 2\varepsilon^2 \left[ \frac{g(1 + e^{-x_0/\varepsilon})}{x_0} + \frac{g(1 + e^{-(1-x_0)/\varepsilon})}{1-x_0} \right] \right\} dt \\
&\sim \int_0^t \left\{ -\frac{\pi^2 \varepsilon^2}{6x_0(1-x_0)} + \varepsilon(\log 4 - 1) + \frac{1}{2}x_0^2 - \frac{1}{2}x_0 + \frac{1}{6} \right\} dt. \tag{5.5b}
\end{aligned}$$

Here  $g(x) \equiv \int_0^x \frac{\log t}{1-t} dt$ , which satisfies  $g(x) \sim 1-x$  as  $x \rightarrow 1$ . To determine  $y(x, t)$  during the metastable evolution we solve the ODE (4.19) numerically and obtain  $h(t)$  from a numerical quadrature. Equation (5.5a) then yields  $y(x, t)$ .

In Fig. 1 and Fig. 10 we plot the metastable solution  $y(x, t)$  versus  $x$  with  $\varepsilon = 0.0115$  and  $\varepsilon = 0.006$ , respectively, at several values of  $t$ . For the example in Fig. 1 it takes a time  $t \approx 117.1$  for the tip of the parabola to move from its initial position  $x_0^0 = 0.45$  to its final equilibrium state at  $x_0 = 0$ . The height  $h(t)$  of the parabola increases by roughly 5.86 during this evolution. A similar observation was observed in the numerical computations of [12] (see Fig. 3 of [12]). When  $\varepsilon$  is decreased, the height  $h(t)$  can increase dramatically as shown in Fig. 10. This can be explained from (5.5b) since for  $\varepsilon \rightarrow 0$

$$h(t) \sim \int_0^t \left( \frac{1}{2}x_0^2 - \frac{1}{2}x_0 + \frac{1}{6} \right) dt \geq \frac{1}{24}t. \tag{5.6}$$

## Acknowledgements

M.J.W. would like to thank Prof. S. Kamin and Prof. H. Berestycki for introducing us to this problem.

$x_0$	t(num.)	t(asy.)
0.3999931	$0.131068167 \times 10^6$	$0.133057866 \times 10^6$
0.3999216	$0.149606553 \times 10^7$	$0.151644288 \times 10^7$
0.3983913	$0.277759851 \times 10^8$	$0.281609517 \times 10^8$
0.3904987	$0.103529490 \times 10^9$	$0.105057930 \times 10^9$
0.3750825	$0.140377491 \times 10^9$	$0.142599219 \times 10^9$
0.3202282	$0.146999074 \times 10^9$	$0.149374926 \times 10^9$
0.2574865	$0.147019482 \times 10^9$	$0.149396440 \times 10^9$
0.2020624	$0.147019608 \times 10^9$	$0.149396594 \times 10^9$
0.0898295	$0.147019614 \times 10^9$	$0.149396603 \times 10^9$

Table 7: A comparison of the asymptotic and numerical results for  $t = t(x_0)$  for the asymmetric  $f(u)$  of (5.2) with  $\varepsilon = 0.004$  and  $x_0^0 = 0.4$ .

## A Estimating the weight function $\omega$

For  $\varepsilon \rightarrow 0$ , we now calculate the weight function  $\omega(x)$ , defined in (2.18), in both the outer and the boundary layer regions. In the outer region we use  $\tilde{u}^\varepsilon = x - x_0 + \text{t.s.t}$  to obtain

$$\omega(x) = \exp[-f(x - x_0)/\varepsilon](1 + \text{t.s.t.}) . \quad (0.1)$$

In the left boundary layer near  $x = 0$  we first integrate (2.3a) to get

$$u'_{l_0}(y) \exp\left(-\int_0^y f'[-x_0 + u_{l_0}(z)] dz\right) = u'_{l_0}(0), \quad \text{for } 0 < y < \infty . \quad (0.2)$$

Then, we re-write  $\omega(x)$  exactly as

$$\omega(x) = \omega(0) \exp\left(-\varepsilon^{-1} \int_0^x f'[\tilde{u}^\varepsilon(z)] dz\right) . \quad (0.3)$$

Let  $y = x/\varepsilon$  and use  $\tilde{u}^\varepsilon(x) \sim -x_0 + u_{l_0}(\varepsilon^{-1}x)$  in (0.3) to get

$$\omega(\varepsilon y) \sim \omega(0) \exp\left(-\int_0^y f'[-x_0 + u_{l_0}(z)] dz\right) . \quad (0.4)$$

Comparing (0.4) with (0.2) we observe that  $\omega(\varepsilon y)u'_{l_0}(y)$  is asymptotically constant and, hence,

$$\omega(\varepsilon y)u'_{l_0}(y) \sim \omega(0)u'_{l_0}(0) \quad (0.5)$$

To calculate  $\omega(0)u'_{l_0}(0)$  we evaluate the left side of (0.5) as  $y \rightarrow \infty$  using (0.1) and the decay behavior (2.3b) for  $u_{l_0}$ . This yields the key identity

$$\omega(0)u'_{l_0}(0) \sim -a_{l_0}\nu_l \exp(-f(-x_0)/\varepsilon) , \quad (0.6)$$

$x_0$	t(num.)	t(asy.)
0.3499993	$0.112330078 \times 10^5$	$0.111349461 \times 10^5$
0.3499269	$0.132980269 \times 10^7$	$0.134879406 \times 10^7$
0.3493105	$0.120121899 \times 10^8$	$0.121708663 \times 10^8$
0.3476808	$0.359540384 \times 10^8$	$0.364335772 \times 10^8$
0.3380873	$0.102874830 \times 10^9$	$0.104310107 \times 10^9$
0.3005508	$0.126006321 \times 10^9$	$0.127873597 \times 10^9$
0.2503833	$0.126203956 \times 10^9$	$0.128078207 \times 10^9$
0.2012807	$0.126205089 \times 10^9$	$0.128079463 \times 10^9$
0.0884271	$0.126205114 \times 10^9$	$0.128079498 \times 10^9$

Table 8: A comparison of the asymptotic and numerical results for  $t = t(x_0)$  for the asymmetric  $f(u)$  of (5.2) with  $\varepsilon = 0.003$  and  $x_0^0 = 0.35$ .

where  $a_{l_0}$  and  $\nu_l$  are defined in (2.5).

A similar analysis, which we shall omit, can be done in the right boundary layer region near  $x = 0$  to show that the product  $\omega(1 - \varepsilon y)u'_{r_0}(y)$  is asymptotically constant in this region. The key identity, analogous to (0.6), is that

$$\omega(1 - \varepsilon y)u'_{r_0}(y) \sim \omega(1)u'_{r_0}(0) \sim a_{r_0} \nu_r \exp(-f(1 - x_0)/\varepsilon), \quad (0.7)$$

where  $a_{r_0}$  and  $\nu_r$  are defined in (2.10).

## References

- [1] U. Ascher, R. Christiansen, R. Russell, *Collocation software for boundary value ODE's*, Math. Comp. **33**, (1979), pp. 659–679.
- [2] U. Ascher, R. Robert, R. Russell, *Numerical solution of boundary value problems for ordinary differential equations*. Englewood Cliffs, N.J., Prentice Hall, 1988.
- [3] P.B. Bailey, M.K. Gordon, L.F. Shampine, *Automatic solution of the Sturm–Liouville problem*, ACM Trans. on Math. Software **4**, (1978), pp. 193–208.
- [4] H. Berestycki, S. Kamin, G. Sivashinsky, *Nonlinear dynamics and metastability in a Burgers type equation*, Comptes Rendus Acad. Sci., Paris t. **321**, Série 1, (1995), pp. 185–190.
- [5] J. Carr, R. Pego, *Metastable patterns in solutions of  $u_t = \varepsilon^2 u_{xx} - f(u)$* , Comm. Pure Appl. Math. **42**, (1989), pp. 523–576.

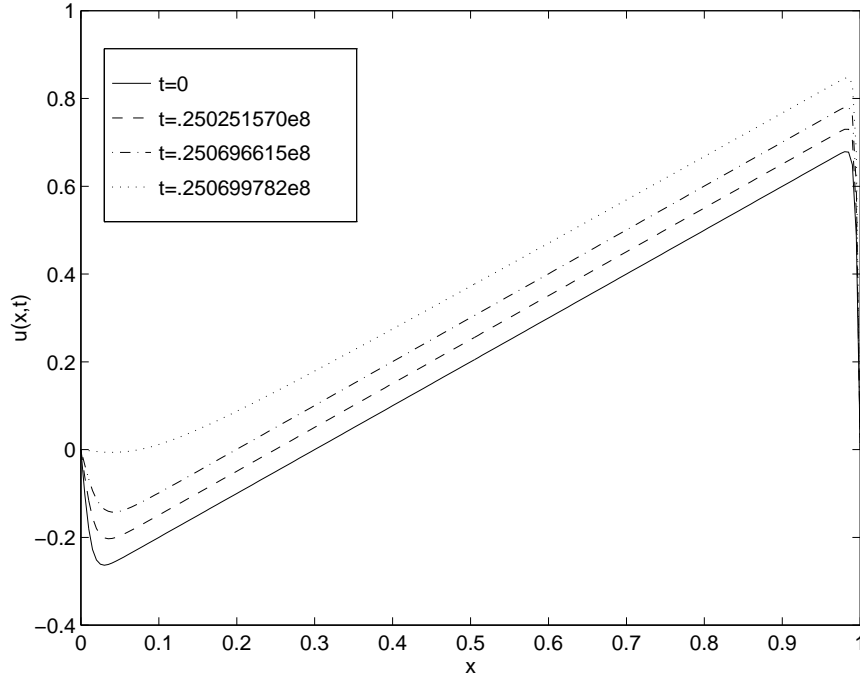


Figure 6: Plot of the numerical solution to (1.2) at different times. Here  $\varepsilon = 0.002$  and  $x_0^0 = 0.3$ .

- [6] G. Fusco, J.K. Hale, *Slow motion manifolds, dormant instability and singular perturbations*, J. Dyn. Diff. Equat. **1**, (1989), pp. 75–94.
- [7] I. Gladwell, K.K. Sayers, *Computational techniques for ordinary differential equations*, Academic Press, London, 1980.
- [8] J. Goodman, *Stability of the Kuramoto-Sivashinsky and related systems*, Comm. Pure Appl. Math. **47**, (1994), pp. 293–306.
- [9] M.E. Hosea, L.F. Shampine, *Global extrapolation integrators for solving Sturm-Liouville problems by shooting*, IMA J. Numer. Anal. **13**, (1993), pp. 397–411.
- [10] J. Laforgue, R.E. O’Malley, *On the motion of viscous shocks and the super-sensitivity of their steady-state limits*, Methods and Appl. of Anal. **1**, (1994), pp. 465–487.
- [11] J. Lee, M.J. Ward, *On the asymptotic and numerical analyses of exponentially ill-conditioned singularly perturbed boundary value problems*, Stud. Appl. Math. **94**, (1995), pp. 271–326.

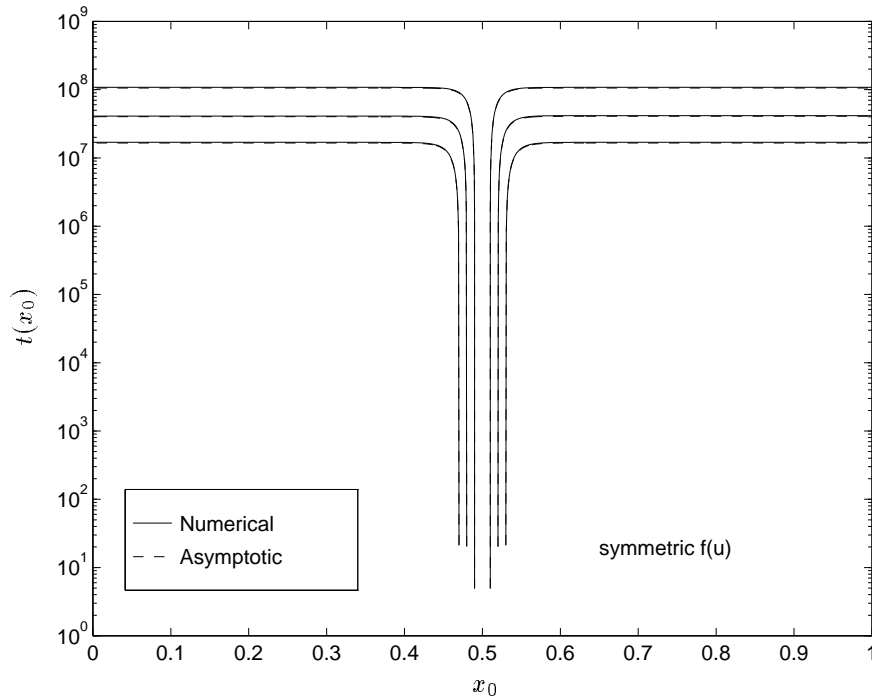


Figure 7: Plots of asymptotic and numerical results for the tip location  $t = t(x_0)$  of the parabolic-shaped flame-front interface for (1.2) with  $\varepsilon = 0.005$ . A logarithmic (base 10) scale is used for the vertical axis.

- [12] A.B. Mikishev, G.I. Sivashinsky, *Quasi-equilibrium in upward propagating flames*, Physics Letters A, **175**, (1993), pp. 409–414.
- [13] Z. Rakib, G.I. Sivashinsky, *Instabilities in upward propagating flames*, Combust. Sci. and Tech. **54**, (1987), pp. 69–84.
- [14] L.G. Reyna, M.J. Ward, *On the exponentially slow motion of a viscous shock*, Comm. Pure Appl. Math. **48**, (1995), pp. 79–120.
- [15] M.J. Ward, *Metastable patterns, layer collapses, and coarsening for a one-dimensional Ginzburg-Landau equation*, Stud. Appl. Math. **91**, (1994), pp. 51–93.
- [16] M.J. Ward, *Dynamic metastability and singular perturbations*, submitted 1/96, AMS proceedings of CRM sponsored Banff conference on ‘Boundaries, Interfaces and Transitions’.

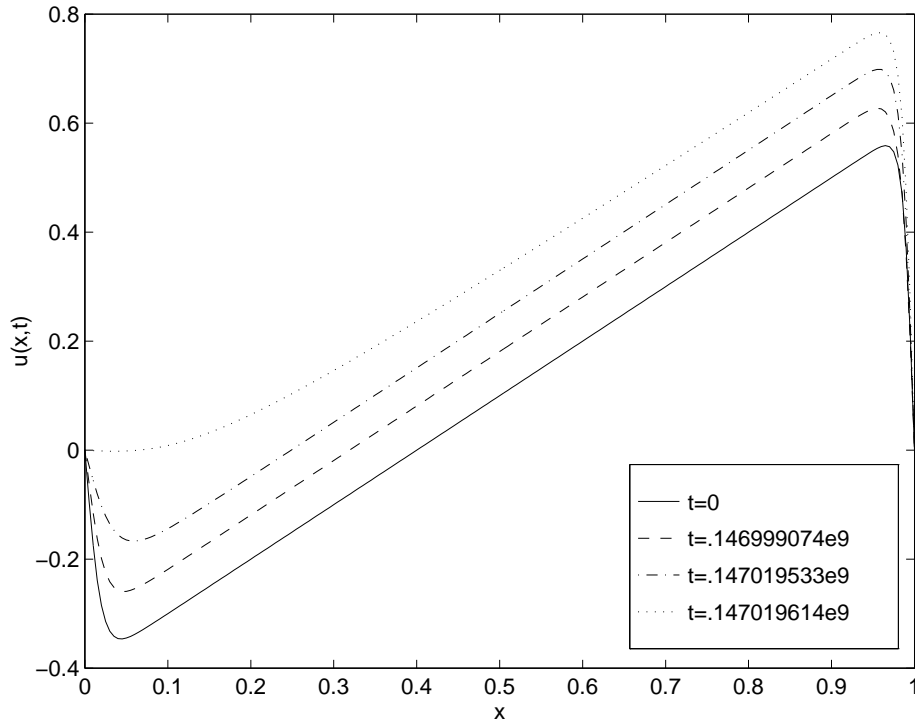


Figure 8: Plot of the numerical solution to (1.7) with the asymmetric  $f(u)$  of (5.2) at different times. Here  $\varepsilon = 0.004$ , and  $x_0^0 = 0.4$ .

$\varepsilon$	$x_0^m$ (asy.)	$x_0^m$ (num.)
0.004	0.4412712	0.4412866
0.005	0.4420214	0.4420579
0.006	0.4427894	0.4428554
0.007	0.4435751	0.4436858
0.008	0.4443787	0.4445542
0.009	0.4452002	0.4454679
0.010	0.4460395	0.4464367
0.011	0.4468968	0.4474730
0.012	0.4477721	0.4485919
0.013	0.4486654	0.4498109

Table 9: The equilibrium location of  $x_0^m$  for the asymmetric  $f(u)$  of (5.2).

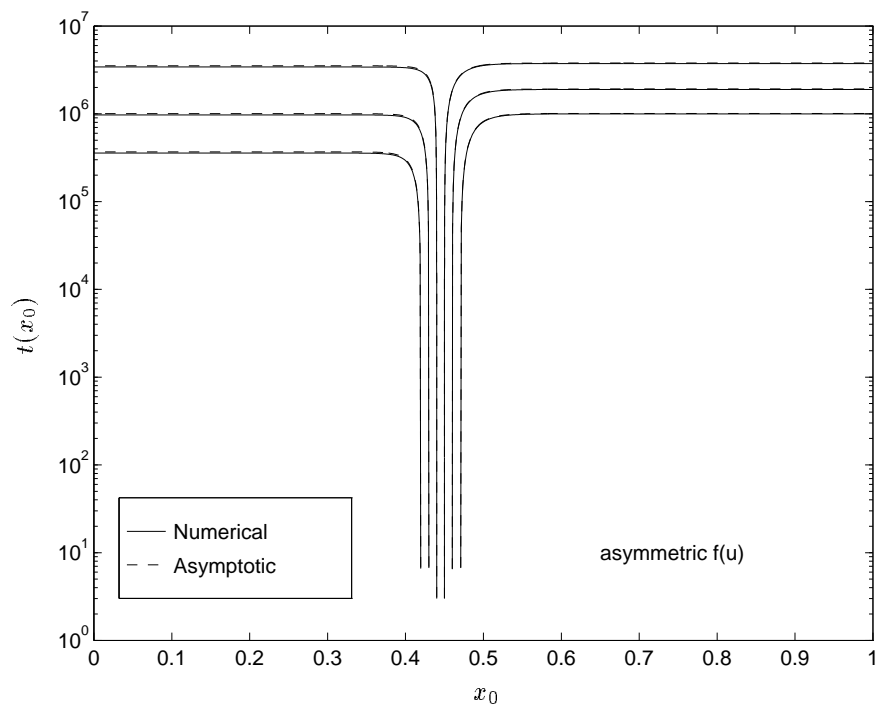


Figure 9: Plots of asymptotic and numerical results for  $t = t(x_0)$  for (1.7) with the asymmetric  $f(u)$  of (5.2) with  $\varepsilon = 0.006$ . A logarithmic (base 10) scale is used for the vertical axis.

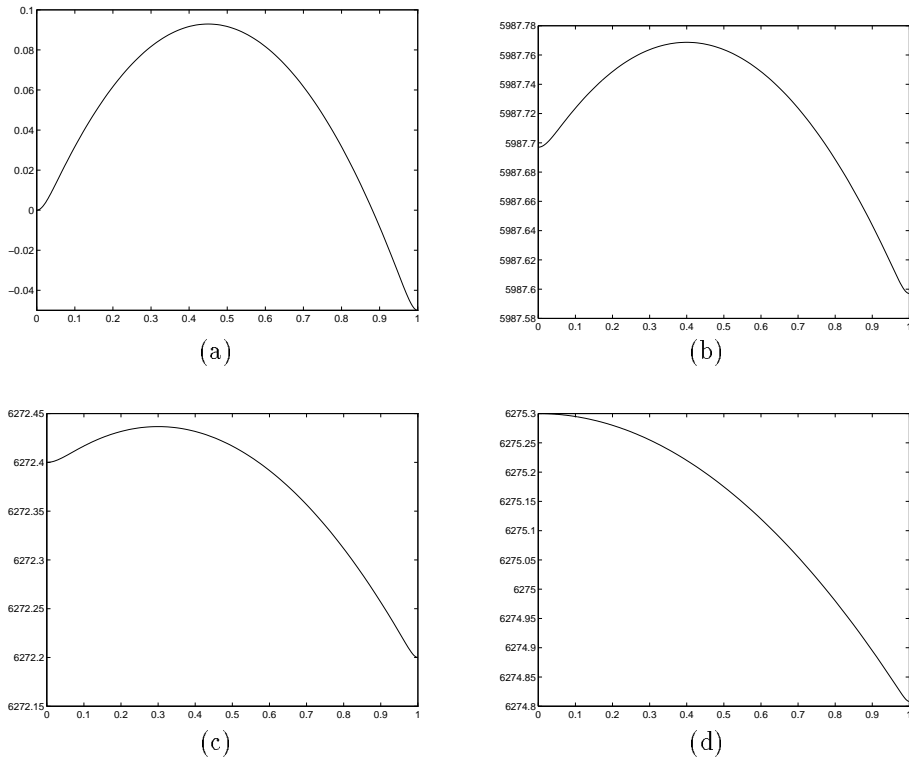


Figure 10: Plot of  $y(x, t)$  versus  $x$  given by (5.5) with  $\varepsilon = .006$  that approximates the metastable behavior in (1.1). (a) initial quasi-equilibrium solution  $y(x, t)$  with tip location  $x_0 = 0.45$  at  $t = 0$ ; (b) quasi-equilibrium solution with  $x_0 = 0.4$  at  $t = 130745$ ; (c) quasi-equilibrium solution with  $x_0 = 0.3$  at  $t = 136353$ ; (d) final stable equilibrium solution at  $t \geq 136394$ .